Photodissociation and geminate recombination dynamics of iodine (I2-) in mass-selected iodine-carbon dioxide (I2-(CO2)n) cluster ions

ARTICLE *in* THE JOURNAL OF PHYSICAL CHEMISTRY · OCTOBER 1991

Impact Factor: 2.78 · DOI: 10.1021/j100174a008

6 AUTHORS, INCLUDING:

Nancy E Levinger
Colorado State University
95 PUBLICATIONS **4,693** CITATIONS

SEE PROFILE

Douglas Ray
Pacific Northwest National Laboratory
32 PUBLICATIONS **1,820** CITATIONS

SEE PROFILE

Vasil Vorsa
Greene Tweed Inc.
18 PUBLICATIONS **527** CITATIONS

SEE PROFILE

Photodissociation and Geminate Recombination Dynamics of I_2^- in Mass-Selected $I_2^-(CO_2)_n$ Cluster Ions

John M. Papanikolas, James R. Gord, Nancy E. Levinger,† Douglas Ray,‡ Vasil Vorsa, and W. C. Lineberger*

Department of Chemistry and Biochemistry, University of Colorado, and Joint Institute for Laboratory Astrophysics, University of Colorado and National Institute of Standards and Technology, Boulder, Colorado 80309 *(Received: February 13, 1991)*

We report size-dependent photodissociation and geminate recombination dynamics of the I_2^- chromophore in mass-selected $I_2^-(CO_2)_n$ cluster ions, $0 \le n \le 22$, by using nanosecond and picosecond pulsed laser sources in conjunction with a tandem time-of-flight mass spectrometer. Photoexcitation of these cluster ions results in the formation of two types of photofragment ions: I_2^--based photofragment ions, in which the photodissociated I_2^- chromophore has recombined and vibrationally relaxed, and I^--based photofragment ions, in which an iodine atom has escaped the cluster ion. The "caging fraction", or quantum yield for formation of photofragment ions containing recombined I_2^-, is strongly dependent on the cluster ion size, varying from zero to unity over the size range studied. Picosecond pump–probe studies reveal a transient bleach in the sequential two-photon absorption of these $I_2^-(CO_2)_n$ cluster ions. A single laser pulse time-resolved experiment indicates that the time scale for absorption recovery is ≈30 ps for cluster ions with $9 \le n \le 13$ and ≈15 ps for $n = 15$ and 16, with a dramatic decrease in absorption recovery time over the size range $13 \le n \le 15$. These results are interpreted in terms of recent Monte Carlo simulations performed in this laboratory and molecular dynamics studies performed by Amar and Perera.

I. Introduction

The rapidly expanding field of cluster research is emerging as an ideal forum for the application of powerful experimental and theoretical techniques to chemical problems of increasing complexity.[1-7] Clusters are sufficiently small that they remain theoretically tractable and can be studied by using sophisticated molecular beam and laser spectroscopic techniques. At the same time, they are sufficiently complex that they provide insight into the forces that govern the physics and chemistry of condensed phases. One particularly powerful application of clusters is in the study of chemical reaction dynamics. Clusters permit us to observe reactions in carefully controlled environments in which the effects of reagent orientation and stepwise solvation on the reaction dynamics can be elucidated. In this paper, we report our studies of size effects on I_2^- photodissociation and geminate recombination in large clusters of CO_2.

Garvey and Bernstein were among the first researchers to investigate intracluster chemical reactions.[8-10] A number of other groups have also carried out pioneering studies of reaction dynamics in neutral and ionic clusters.[11-32] For example, dynamical stereochemistry of reactions has been studied through preparation of complexes and clusters in which reagent orientation is controlled.[23,24] Several groups have pursued the study of photoinitiated chemical reactions in clusters, and their results appear to be particularly promising. Castleman and co-workers have identified a number of intracluster ion–molecule reactions occurring following photoionization.[1,6,11-17] Photoinduced charge transfer in $CO_2O_2^+$ has been observed by Kim et al.[25] The Leutwyler group has carried out photoinduced proton-transfer experiments on 1- and 2-naphthol in clusters of various solvents including NH_3, H_2O, D_2O, CH_3OH, and piperidine.[26-30] Their results dramatically demonstrate the effects of stepwise solvation on proton transfer. In this laboratory, we have investigated size effects in the recombination of photodissociated dihalogens in cluster ions.[31,32]

Very recently, the area of intracluster reaction dynamics has benefited from ultrafast spectroscopic techniques[33] which are revolutionizing the investigation of solvent dynamics in condensed phases[34,35] and of isolated dissociative half-collisions and bimolecular reactions in the gas phase.[36,37] The Syage group has employed picosecond pump–probe spectroscopy to study photoinduced proton transfer in phenol$(NH_3)_n$ clusters[38] and to investigate ladder switching and ladder climbing mechanisms in the formation of photofragment ions from $(CH_3I)_n$ clusters.[39] Breen

†Present address: Department of Chemistry, University of Minnesota, Minneapolis, MN 55455.

‡Present address: Molecular Science Research Center, K2-18, Pacific Northwest Laboratory, P.O. Box 999, Richland, WA 99352.

(1) Castleman, A. W., Jr. In *Clusters of Atoms and Molecules*; Haberland, H., Ed.; Springer-Verlag: New York, submitted for publication.
(2) Duncan, M. A.; Rouvray, D. H. *Sci. Am.* **1989**, *261*, 110.
(3) Buckner, S. W.; Freiser, B. S. In *Gas Phase Inorganic Chemistry*; Russell, D. H., Ed.; Plenum Press: New York, 1988.
(4) Campana, J. E. *Mass Spectrom. Rev.* **1987**, *6*, 395.
(5) Morse, M. D. *Chem. Rev.* **1986**, *86*, 1049.
(6) Castleman, A. W., Jr.; Keesee, R. G. *Chem. Rev.* **1986**, *86*, 589.
(7) Smalley, R. E. *Laser Chem.* **1983**, *2*, 167.
(8) Garvey, J. F.; Bernstein, R. B. *J. Am. Chem. Soc.* **1986**, *108*, 6096.
(9) Garvey, J. F.; Bernstein, R. B. *J. Phys. Chem.* **1986**, *90*, 3577.
(10) Garvey, J. F.; Bernstein, R. B. *Chem. Phys. Lett.* **1986**, *126*, 394.
(11) Märk, T. D.; Castleman, A. W., Jr. In *Advances in Atomic and Molecular Physics*; Academic Press: New York, 1985; Vol. 20.
(12) Echt, O.; Dao, P. D.; Morgan, S.; Castleman, A. W., Jr. *J. Chem. Phys.* **1985**, *82*, 4076.
(13) Castleman, A. W., Jr.; Echt, O.; Morgan, S.; Dao, P. D. *Ber. Bunsen-Ges. Phys. Chem.* **1985**, *89*, 281.
(14) Echt, O.; Stanley, R. J.; Dao, P. D.; Castleman, A. W., Jr. *Ber. Bunsen-Ges. Phys. Chem.* **1984**, *88*, 217.
(15) Hermann, V.; Key, B. D.; Castleman, A. W., Jr. *Chem. Phys.* **1982**, *72*, 185.
(16) Stephan, K.; Futrell, J. H.; Peterson, K. I.; Castleman, A. W., Jr.; Wagner, H. E.; Djuric, N.; Mark, T. D. *Int. J. Mass Spectrom. Ion Phys.* **1982**, *44*, 167.
(17) Stephan, K.; Futrell, J. H.; Peterson, K. I.; Castleman, A. W., Jr.; Märk, T. D. *J. Chem. Phys.* **1982**, *77*, 2408.
(18) Klots, C. E.; Compton, R. N. *J. Chem. Phys.* **1978**, *69*, 1644.
(19) Klots, C. E.; Compton, R. N. *J. Chem. Phys.* **1978**, *69*, 1636.
(20) Ceyer, S. T.; Tiedemann, P. W.; Mahan, B. H.; Lee, Y. T. *J. Chem. Phys.* **1979**, *70*, 2138.
(21) Ceyer, S. T.; Tiedemann, P. W.; Mahan, B. H.; Lee, Y. T. *J. Chem. Phys.* **1979**, *70*, 14.
(22) Milne, T. A.; Beachey, J. E.; Greene, F. T. Air Force Cambridge Research Laboratories, 1970; AFCR L-70-0341.
(23) Wittig, C.; Sharpe, S.; Beaudet, R. A. *Acc. Chem. Res.* **1988**, *21*, 341.
(24) Dynamical Stereochemistry Issue. *J. Phys. Chem.* **1987**, *91*, 5365-5509.
(25) Kim, H.-S.; Kuo, C.-H.; Bowers, M. T. *J. Chem. Phys.* **1987**, *87*, 2667.
(26) Droz, T.; Knochenmuss, R.; Leutwyler, S. *J. Chem. Phys.* **1990**, *93*, 4520.
(27) Knochenmuss, R.; Leutwyler, S. *J. Chem. Phys.* **1989**, *91*, 1268.
(28) Cheshnovsky, O.; Leutwyler, S. *J. Chem. Phys.* **1988**, *88*, 4127.
(29) Knochenmuss, R.; Cheshnovsky, O.; Leutwyler, S. *Chem. Phys. Lett.* **1988**, *144*, 317.
(30) Cheshnovsky, O.; Leutwyler, S. *Chem. Phys. Lett.* **1985**, *121*, 1.
(31) Alexander, M. L.; Levinger, N. E.; Johnson, M. A.; Ray, D.; Lineberger, W. C. *J. Chem. Phys.* **1988**, *88*, 6200.
(32) Levinger, N. E. Ph.D. Thesis, University of Colordao at Boulder, May 1990.
(33) Fleming, G. R. *Chemical Applications of Ultrafast Spectroscopy*; Oxford University Press: New York, 1986.
(34) Barbara, P. F.; Jarzeba, W. *Acc. Chem. Res.* **1988**, *21*, 195.

0022-3654/91/2095-8028$02.50/0

et al. have studied, on the picosecond time scale, the effects of stepwise solvation on proton transfer in small 1-naphthol$(NH_3)_n$ clusters.[40] They have also reported state-to-state rates for vibrational and electronic predissociation in I_2Ar.[41] Finally, a preliminary report from this laboratory describes the use of picosecond pump–probe techniques to study recombination and vibrational relaxation of photodissociated I_2^- in $I_2^-(CO_2)_9$ and $I_2^-(CO_2)_{16}$ cluster ions.[42]

For the interpretation of these types of experiments to be unambiguous, initial size selection of the precursor cluster is crucial. Often small neutral clusters and van der Waals complexes generated in supersonic expansions can be size selected on the basis of their spectroscopic signatures. Buck and co-workers have developed an ingenious approach to neutral cluster size selection which employs molecular beam scattering.[43] However, selection is most readily accomplished through the use of charged clusters, which can be prepared with controlled size and composition and then selected by using mass spectrometric techniques. Several types of instrumentation have been developed for the study of size-selected cluster ions[44-52] including tandem time-of-flight (TOF)[31,53-58] and Fourier transform ion cyclotron resonance (FTICR)[59-63] mass spectrometers.

Our interest in the effects of stepwise solvation on intracluster chemical reaction dynamics has prompted us to study one of the classic processes in physical chemistry, namely photodissociation and geminate recombination of diatomic halogens. Since the seminal efforts of Franck, Rabinowitch, and Wood,[64-66] these

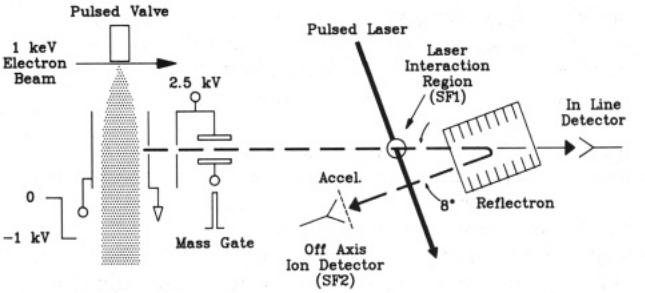

Figure 1. Schematic representation of the cluster ion source and tandem time-of-flight mass spectrometer. Small anions generated in the source by interaction of a 1-keV electron beam with a pulsed supersonic expansion grow by accretion. These ions are injected into the primary TOF by using a pulsed electric field. The ions interact with a pulsed laser at the first spatial focus (SF1). Photofragment ions and parent ions are mass analyzed in a single field reflectron and then accelerated into a particle multiplier located at the second spatial focus (SF2). Species that traverse the reflectron strike the in-line detector.

systems have been a major testing ground for probing the role of the solvent in chemical reactions. Photolysis experiments and theoretical simulations performed for Cl_2, Br_2, and I_2 in liquids[67-71] and gases[72-77] indicate that quantum yields for recombination of the nascent halogen atoms are dictated by the initial interaction with the "solvent cage". In addition, photoemission experiments[78-87] and simulations[88] in rare-gas matrices demonstrate that the size of the solvent cage surrounding the dihalogen affects its recombination after photodissociation.

A new dimension in the study of recombination dynamics has come during the past two decades with the application of ultrafast spectroscopy to the photodissociation/geminate recombination of dihalogens in condensed phases.[89] Picosecond pump–probe experiments have demonstrated that geminate recombination of photodissociated I_2 takes place in ≤ 2 ps, while subsequent vibrational relaxation of the recombined I_2 chromophore occurs on a time scale ranging from 50 ps to several nanoseconds, depending on the solvent.[90-100] Isolated binary collision models[90,101] and full

(35) Simon, J. D. *Acc. Chem. Res.* **1988**, *21*, 128.
(36) Zewail, A. H. *Science* **1988**, *242*, 1645.
(37) Zewail, A. H.; Bernstein, R. B. *Chem. Eng. News* **1988**, *66*, 24.
(38) Steadman, J.; Syage, J. A. *J. Chem. Phys.* **1990**, *92*, 4630.
(39) Steadman, J.; Fournier, E. W.; Syage, J. A. *Appl. Opt.* **1990**, *29*, 4962.
(40) Breen, J. J.; Peng, L. W.; Willberg, D. M.; Heikal, A.; Cong, P.; Zewail, A. H. *J. Chem. Phys.* **1990**, *92*, 805.
(41) Breen, J. J.; Willberg, D. M.; Gutmann, M.; Zewail, A. H. *J. Chem. Phys.* **1990**, *93*, 9180.
(42) Ray, D.; Levinger, N. E.; Papanikolas, J. M.; Lineberger, W. C. *J. Chem. Phys.* **1989**, *91*, 6533.
(43) Buck, U. *J. Phys. Chem.* **1988**, *92*, 1023.
(44) Jarrold, M. F.; Bower, J. E.; Creegan, K. *J. Chem. Phys.* **1989**, *90*, 3615.
(45) Okumura, M.; Yeh, L. I.; Lee, Y. T. *J. Chem. Phys.* **1988**, *88*, 79.
(46) Shul, R. J.; Upschulte, B. L.; Passarella, R.; Keesee, R. G.; Castleman, A. W., Jr. *J. Phys. Chem.* **1987**, *91*, 2556.
(47) Leopold, D. G.; Ho, J.; Lineberger, W. C. *J. Chem. Phys.* **1987**, *86*, 1715.
(48) Hanley, L.; Ruatta, S. A.; Anderson, S. L. *J. Chem. Phys.* **1987**, *87*, 260.
(49) David, D. E.; Magnera, T. F.; Tian, R.; Stulik, D.; Michl, J. *Nucl. Instrum. Methods Phys. Res. B* **1986**, *B14*, 378.
(50) Ervin, K. M.; Armentrout, P. B. *J. Chem. Phys.* **1985**, *83*, 166.
(51) Hunton, D. E.; Hofmann, M.; Lindeman, T. G.; Castleman, A. W., Jr. *J. Chem. Phys.* **1985**, *82*, 134.
(52) Fayet, P.; Wöste, L. *Surf. Sci.* **1985**, *156*, 134.
(53) Nagata, T.; Hirokawa, J.; Ikegami, T.; Kondow, T.; Iwata, S. *Chem. Phys. Lett.* **1990**, *171*, 433.
(54) LaiHing, K.; Cheng, P. Y.; Taylor, T. G.; Willey, K. F.; Peschke, M.; Duncan, M. A. *Anal. Chem.* **1989**, *61*, 1458.
(55) Posey, L. A.; Johnson, M. A. *J. Chem. Phys.* **1988**, *89*, 4807.
(56) Bréchignac, C.; Cahuzac, Ph.; Toux, J.-Ph. *J. Chem. Phys.* **1988**, *88*, 3022.
(57) Geusic, M. E.; Jarrold, M. F.; McIlrath, T. J.; Freeman, R. R.; Brown, W. L. *J. Chem. Phys.* **1987**, *86*, 3862.
(58) Brucat, P. J.; Zheng, L.-S.; Pettiette, C. L.; Yang, S.; Smalley, R. E. *J. Chem. Phys.* **1986**, *84*, 3078.
(59) Buckner, S. W.; Gord, J. R.; Freiser, B. S. *J. Chem. Phys.* **1988**, *88*, 3678.
(60) Jacobson, D. B. *J. Am. Chem. Soc.* **1987**, *109*, 6851.
(61) Moini, M.; Eyler, J. R. *Chem. Phys. Lett.* **1987**, *137*, 311.
(62) Mandich, M. L.; Bondybey, V. E.; Reents, W. D., Jr. *J. Chem. Phys.* **1987**, *86*, 4245.
(63) Alford, J. M.; Williams, P. E.; Trevor, D. J.; Smalley, R. E. *Int. J. Mass Spectrom. Ion Processes* **1986**, *72*, 33.
(64) Rabinowitch, E.; Wood, W. C. *Trans. Faraday Soc.* **1936**, *32*, 1381.
(65) Rabinowitch, E.; Wood, W. C. *Trans. Faraday Soc.* **1936**, *32*, 547.
(66) Franck, J.; Rabinowitch, E. *Trans. Faraday Soc.* **1934**, *30*, 120.
(67) Dardi, P. S.; Dahler, J. S. *J. Chem. Phys.* **1990**, *93*, 242.
(68) Otto, B.; Schroeder, J.; Troe, J. *J. Chem. Phys.* **1984**, *81*, 202.
(69) Luther, K.; Schroeder, J.; Troe, J.; Unterberg, U. *J. Phys. Chem.* **1980**, *84*, 3072.
(70) Meadows, L.; Noyes, R. M. *J. Am. Chem. Soc.* **1960**, *82*, 1872.
(71) Booth, D.; Noyes, R. M. *J. Am. Chem. Soc.* **1960**, *82*, 1868.
(72) Hippler, H.; Schuebert, V.; Troe, J. *J. Chem. Phys.* **1984**, *81*, 3931.
(73) Dutoit, J. C.; Zellweger, J. M.; van den Bergh, H. *J. Chem. Phys.* **1983**, *78*, 1825.
(74) Zellweger, J. M.; van den Bergh, H. *J. Chem. Phys.* **1980**, *72*, 5405.
(75) Luther, K.; Troe, J. *Chem. Phys. Lett.* **1974**, *24*, 85.
(76) Hippler, H.; Luther, K.; Troe, J. *Ber. Bunsen-Ges. Phys. Chem.* **1973**, *77*, 1104.
(77) Hippler, H.; Luther, K.; Troe, J. *Chem. Phys. Lett.* **1972**, *16*, 174.
(78) Kunz, H.; McCaffrey, J. G.; Schriever, R.; Schwentner, N. *J. Chem. Phys.* **1991**, *94*, 1039.
(79) Beeken, P. B.; Hanson, E. A.; Flynn, G. W. *J. Chem. Phys.* **1983**, *78*, 5892.
(80) Beeken, P.; Mandich, M.; Flynn, G. *J. Chem. Phys.* **1982**, *76*, 5995.
(81) Mandich, M.; Beeken, P.; Flynn, G. *J. Chem. Phys.* **1982**, *77*, 702.
(82) Bondybey, V. E.; Brus, L. E. *Adv. Chem. Phys.* **1980**, *41*, 269.
(83) Bondybey, V. E.; Bearder, S. S.; Fletcher, C. *J. Chem. Phys.* **1976**, *64*, 5243.
(84) Bondybey, V. E.; Brus, L. E. *J. Chem. Phys.* **1976**, *64*, 3724.
(85) Bondybey, V. E.; Fletcher, C. *J. Chem. Phys.* **1976**, *64*, 3615.
(86) Bondybey, V. E.; Brus, L. E. *J. Chem. Phys.* **1975**, *62*, 620.
(87) Ault, B. S.; Howard, W. F.; Andrews, L. *J. Mol. Spectrosc.* **1975**, *55*, 217.
(88) Alimi, R.; Brokman, A.; Gerber, R. B. *J. Chem. Phys.* **1989**, *91*, 1611.
(89) Harris, A. L.; Brown, J. K.; Harris, C. B. *Annu. Rev. Phys. Chem.* **1988**, *39*, 341.
(90) Paige, M. E.; Harris, C. B. *Chem. Phys.* **1990**, *149*, 37.

molecular dynamics simulations[102] of these systems demonstrate the effects of solvent density on the vibrational relaxation process. The fate of the dissociating I_2 molecules, especially their vibrational relaxation following recombination, is strongly influenced by the local solvent environment.

A number of experiments and simulations[103,104] have addressed solvent effects on dihalogen photodissociation and recombination in clusters. The quantum yield for dissociation of molecular iodine excited above the dissociation limit of its B state is unity.[105] However, several groups have observed $B \rightarrow X$ fluorescence from intact I_2 after excitation above its B-state dissociation limit in clusters with rare-gas atoms[106-110] and in $(I_2)_2$.[111] These studies suggest that even one solvent atom is sufficient to induce caging in these clusters. The size dependence of the caging quantum yield in $Br_2^-(CO_2)_n$ cluster ions has been studied in this laboratory.[31] In addition, we have reported time-resolved studies of recombination in $I_2^-(CO_2)_9$ and $I_2^-(CO_2)_{16}$.[42] Finally, Amar and coworkers have carried out molecular dynamics (MD) simulations of photodissociation and recombination in Br_2Ar_n,[112] $Br_2^-Ar_n$ and $Br_2^-(CO_2)_n$,[113,114] and $I_2^-(CO_2)_n$.[115] These simulations have provided important insights into recombination mechanisms in these systems.

Here we report the photodissociation and geminate recombination dynamics of I_2^- interacting with a specific number of CO_2 molecules. In section II we briefly describe the salient details of the cluster ion source, tandem time-of-flight mass spectrometer, and nanosecond and picosecond laser systems employed in this study. Our results are presented and discussed in section III. We review our major findings and discuss prospects for future experiments in section IV.

II. Experimental Section

A schematic diagram of the experimental apparatus is displayed in Figure 1. A detailed description has appeared elsewhere,[31,32] so only a brief description will be given here. In our ion source, $I_2^-(CO_2)_n$ cluster ions are generated in a pulsed supersonic expansion crossed with a continuous electron beam. Attachment of low-energy secondary electrons to I_2 seeded in the CO_2 expansion produces I_2^-, from which larger cluster ions grow through ion–molecule reactions. A pulsed electric field extracts these large cluster ions from the expansion and accelerates them into a tandem time-of-flight (TOF) mass spectrometer. The first stage of the mass spectrometer, which is of Wiley–McLaren design,[116] separates the cluster ion beam according to mass at the first spatial focus (SF1), where these ions can interact with a pulsed laser. The second stage, which is a single field reflectron,[117] refocuses the beam at the off-axis ion detector located at the second spatial focus (SF2). This tandem TOF mass spectrometer can be operated in three modes: (1) The pulsed laser is gated off, and the reflectron is configured to refocus the primary ion beam at the off-axis detector providing a parent cluster ion mass spectrum. (2) The laser is gated on, and depletion of the parent cluster ion intensity is monitored to measure absolute photodestruction cross sections. (3) The instrument is operated in an MS/MS configuration, in which the reflectron is adjusted to mass analyze the photofragment ions arising from laser excitation of a mass-selected parent cluster ion.

A. Cluster Ion Source and Tandem Time-of-Flight Mass Spectrometer. $I_2^-(CO_2)_n$ cluster ions are generated by passing pure CO_2 at a pressure of 2–3 atm over solid iodine crystals contained in a stainless steel bubbler heated to 70 °C. The resulting gas mixture expands supersonically through a pulsed valve (General Valve Series 9) with a nozzle diameter of 800 μm. The valve body and associated gas-handling system are heated (30–35 °C) to minimize condensation of the entrained iodine vapor. Positive and negative ions (I^-, I_2^-, and small CO_2 anionic clusters) are formed initially in the pulsed free jet expansion when it is crossed with a 1-keV electron beam. The unskimmed expansion drifts for ≈20 cm during which time these ions grow via CO_2 accretion in the ≈20 K CO_2 neutral bath in which they are immersed.[118] After this drift region the density of the expansion is sufficiently low that a pulsed electric field can be used to extract the cluster ions, without significant collisional excitation, into a differentially pumped tandem time-of-flight (TOF) mass spectrometer. The 1-kV extraction pulse, which rises quickly (≈10 ns) and remains on while the ions are in the extraction region, forms the first acceleration stage of a Wiley–McLaren TOF mass spectrometer.[116] After exiting the extraction region, the cluster ions enter a second acceleration stage and receive an additional 2.5 keV of kinetic energy. The ions thus acquire a kinetic energy of 3000 ± 200 eV for TOF mass analysis. The ion kinetic energy spread arises from the spatial extent of the ions in the extraction region.

At the spatial focus of the primary TOF mass spectrometer (SF1), the cluster ions, which are separated in time according to their masses, intersect a pulsed laser beam. Adjustment of the time delay between the extraction pulse and the laser pulse provides for mass-selective excitation. The absorption of a photon by the selected cluster ion results in the generation of ionic and neutral photofragments, which are separated from each other and from the intact parent ions by using a reflection type TOF mass analyzer.[117] Adjustment of the reflectron field allows either the initial parent ion or the ionic photofragments to be refocused at the off-axis detector (SF2) with a mass resolution of ≈150 for parent ions and ≈50 for photofragment ions.[31] When ionic photofragments are refocused at SF2, the reflectron field is insufficient for reversal of the parent ion trajectory. In this mode the parent ions and any neutral photodissociation products traverse the reflectron field and strike the in-line detector.

In some of the experiments, a pulsed mass gate, constructed from two parallel plate deflectors (15 mm long, 5 mm separation) and located upstream of SF1, is used to reject unwanted parent

(91) Lingle, R., Jr.; Xu, X.; Yu, S.-C.; Zhu, H.; Hopkins, J. B. *J. Chem. Phys.* **1990**, *93*, 5667.
(92) Smith, D. E.; Harris, C. B. *J. Chem. Phys.* **1987**, *87*, 2709.
(93) Paige, M. E.; Russell, D. J.; Harris, C. B. *J. Chem. Phys.* **1986**, *85*, 3699.
(94) Harris, A. L.; Berg, M.; Harris, C. B. *J. Chem. Phys.* **1986**, *84*, 788.
(95) Berg, M.; Harris, A. L.; Harris, C. B. *Phys. Rev. Lett.* **1985**, *54*, 951.
(96) Bado, P.; Dupuy, C.; Magde, D.; Wilson, K. R.; Malley, M. M. *J. Chem. Phys.* **1984**, *80*, 5531.
(97) Kelley, D. F.; Abul-Haj, N. A.; Jang, D.-J. *J. Chem. Phys.* **1984**, *80*, 4105.
(98) Bado, P.; Berens, P. H.; Wilson, K. R. *Proc. Soc. Photo-Opt. Instrum. Eng.* **1982**, *322*, 230.
(99) Langhoff, C. A.; Moore, B.; DeMeuse, M. *J. Am. Chem. Soc.* **1982**, *104*, 3576.
(100) Chaung, T. J.; Hoffman, G. W.; Eisenthal, K. B. *Chem. Phys. Lett.* **1974**, *25*, 201.
(101) Nesbitt, D. J.; Hynes, J. T. *J. Chem. Phys.* **1982**, *77*, 2130.
(102) Brown, J. K.; Harris, C. B.; Tully, J. C. *J. Chem. Phys.* **1988**, *89*, 6687.
(103) Beswick, J. A.; Monot, R.; Philppoz, J.-M.; van den Bergh, H. *J. Chem. Phys.* **1987**, *86*, 3965.
(104) NoorBatcha, I.; Raff, L. M.; Thompson, D. L. *J. Chem. Phys.* **1984**, *81*, 5658.
(105) Burde, D. H.; McFarlane, R. A.; Wiesenfeld, J. R. *Phys. Rev. A* **1974**, *10*, 1917.
(106) Philippoz, J.-M.; van den Bergh, H.; Monot, R. *J. Phys. Chem.* **1987**, *91*, 2545.
(107) Philippoz, J.-M.; Monot, R.; van den Bergh, H. *Helv. Phys. Acta* **1986**, *59*, 1089.
(108) Philippoz, J.-M.; Calpini, B.; Monot, R.; van den Bergh, H. *Helv. Phys. Acta* **1985**, *58*, 875.
(109) Valentini, J. J.; Cross, J. B. *J. Chem. Phys.* **1982**, *77*, 572.
(110) Saenger, K. L.; McClelland, G. M.; Herschbach, D. R. *J. Phys. Chem.* **1981**, *85*, 3333.
(111) Philippoz, J.-M.; Monot, R.; van den Bergh, H. *J. Chem. Phys.* **1990**, *92*, 288.
(112) Amar, F. G.; Berne, B. J. *J. Phys. Chem.* **1984**, *88*, 6720.
(113) Perera, L.; Amar, F. G. *J. Chem. Phys.* **1989**, *90*, 7354.
(114) Amar, F. G. In *Physics and Chemistry of Small Clusters*; Jena, P., Rao, B. K., Khanna, S. N., Eds.; Plenum: New York, 1987; p 207.
(115) Amar, F. G.; Perera, L. Proceedings of the 5th International Meeting on Small Particles and Inorganic Clusters. *Z. Phys. D.*, submitted for publication.
(116) Wiley, W. C.; McLaren, I. H. *Rev. Sci. Instrum.* **1955**, *26*, 1150.
(117) Mamyrin, B. A.; Karataev, V. I.; Schmikk, D. V.; Zagulin, V. A. *Sov. Phys.—JETP (Engl. Transl.)* **1973**, *37*, 45.
(118) Johnson, M. A.; Lineberger, W. C. In *Techniques for the Study of Ion Molecule Reactions*; Farrar, J. M., Saunders, W., Jr., Eds.; Wiley: New York, 1988.

ions. The mass-gate deflector plates are situated between a pair of apertures (input diameter 4 mm, output diameter 5 mm). A dc voltage applied to one of the plates establishes a 500 V/cm electric field inside the mass gate causing any ions that enter the mass gate to be deflected out of the primary ion beam path. The electric field can be quickly reduced to zero (open mass gate) and then reestablished 2–5 μs later (closed mass gate). Adjustment of the time between the extraction pulse and the opening of the mass gate allows cluster ions of a specific mass to pass through the mass gate unaffected. Use of the mass gate eliminates all but the cluster ions of interest and reduces the noise on the in-line and off-axis detectors by about a factor of 10.

In front of the off-axis detector is a series of parallel acceleration meshes. A small potential (≈200 V) is applied to the first mesh to discriminate against low-energy electrons. The second mesh accelerates the ions (≈3 keV) to enhance the detection efficiency. For the fragmentation experiments described below, the off-axis detector was a Johnston MM1 particle multiplier. For the cross-section measurements, a channeltron (Galileo 4830G) operated in its analog mode was employed. Picosecond experiments were also performed with this detector, which was operated in its particle counting mode.

In the negative ion mode of operation, the potential on the anode of the off-axis detector can be as high as 10 kV, requiring capacitive coupling of the ion signal to the pulse processing electronics. The signal is first preamplified (Ortec 9301) and then sent to either a transient digitizer/signal averager (Transiac 2001S/4100) or a gated current integrator (LeCroy 2249SG). For particle counting, a 300-MHz discriminator (Phillips Scientific 6904) is inserted after the preamplification step, and the discriminator output is sent to the LeCroy gated integrator. Since the discriminator output pulses are of fixed amplitude and width, the integrated area is proportional to the number of output pulses. Both the current integrator and transient digitizer are under computer control (IBM AT) via a CAMAC interface (DSP 6001 μP-CAMAC CC).

B. Laser System. The experiments described in this study utilized laser pulses of three different durations. Photodestruction cross sections and photofragment ion mass spectra were measured with ≈6-ns laser pulses. Time-resolved pump–probe experiments employed laser pulses of 1–2-ps duration. To elucidate size effects in $I_2^-(CO_2)_n$ photodissociation/recombination dynamics, a single laser pulse with a 16-ps autocorrelation width was used.

Nanosecond laser pulses were generated by using the frequency-doubled output of a Quanta Ray DCR3 Q-switched Nd:YAG laser (30 Hz, filled beam optics, short pulse mode) to pump a Spectra Physics PDL-1 pulsed dye laser. The output of the PDL-1 laser was typically 15 mJ/pulse throughout the near-infrared region with the use of Exciton dyes (LDS690, LDS750, LDS756) as gain media. The laser intensity at the ion interaction region was controlled with neutral density filters.

Picosecond pulses were generated by frequency doubling the 76-MHz output of a Quantronix 416 mode-locked Nd:YAG laser. This produced pulses of 15 nJ at 532 nm with a width of 70 ps. This light was used to pump synchronously a Coherent 702 dye laser. Generation of 1–2-ps pulses at 720 nm for the pump–probe experiment was achieved by using pyridine 2 dye (LDS722) in the gain jet and a saturable absorber (DDI) in a second jet in the dye laser cavity. Omission of the saturable absorber jet produced the longer pulses (16 ps fwhm autocorrelation width) employed in the single-pulse experiments. Wavelength selection was achieved with a two-plate birefringent filter. The output of this dye laser was cavity dumped at 3.8 MHz in order to obtain pulse energies on the order of 10 nJ/pulse. Part of the dye laser output was directed into an Inrad 5-14 quasi-real-time autocorrelator.

A Spectra Physics PDA pulsed dye amplifier pumped with the second harmonic output (170 mJ/pulse) of a Quanta Ray DCR3 Q-switched Nd:YAG laser was used to amplify the picosecond pulses. The input pulses were amplified in four stages with spatial filters after the first two in order to minimize amplified spontaneous emission (ASE). Three stages were contained in the commercial PDA, and the fourth was added externally for further amplification. The first two cells were side pumped, each receiving 8% of the initial pump beam energy, and the last two cells were end pumped, each receiving 42% of the initial pump beam energy. Typical pulse energies of the 30-Hz PDA output at 720 nm were on the order of 1 mJ with LD700 as the PDA gain medium. A saturable filter (RG715) was placed in the PDA output to remove any remaining ASE. ASE levels were typically ≤1% of the total pulse energy. After amplification, the pulses for the single laser pulse experiment (16 ps fwhm autocorrelation width) were sent directly into the mass spectrometer without further manipulation.

In the pump–probe experiment, two amplified 1–2-ps pulses of the same color and energy were generated by beam-splitting the output of the PDA. One beam was sent down a fixed delay line while the other beam was sent down a variable delay line. The two laser pulses were counterpropagated with polarization parallel to the primary ion beam path through the interaction region of the mass spectrometer. Unfortunately, some time resolution was lost in counterpropagation. The 2-mm thickness of the ion beam resulted in an effective time resolution of ≈6 ps for the pump–probe experiment.

The pump–probe laser pulses were characterized with a noncollinear slow scan autocorrelator. The two pulses were focused onto a 1-mm-thick KDP crystal cut at 48.3°. Second harmonic generation, detected by a PMT, occurred with spatial and temporal overlap of the two beams. Data for the slow scan autocorrelation yielded a pulse width of ≤2 ps (fwhm).

III. Results and Discussion

A. $I_2^-(CO_2)_n$ Cluster Ion Characterization. Clusters and van der Waals complexes generated in free and skimmed supersonic expansions are often ionized during subsequent study, and the resulting ion distribution reflects the possible fragmentation of the neutral precursors.[43,119,120] Since we are interested in studying the ions themselves, we can choose an ion source that minimizes this issue and provides control over the ion chemistry. In our ion source, cluster ions grow directly in the expansion, where they are subject to extensive cooling through stabilizing collisions and evaporation. This drift source is described in more detail below.

A beam of high-energy electrons passes through the dense region of the supersonic expansion, creating a neutral plasma of small positively charged ions and low-energy secondary electrons through ionizing collisions. Attachment of these low-energy electrons to individual molecules or small neutral clusters, via dissociative or evaporative attachment,[18,19] produces small negatively charged "seed" ions. These ions react and grow within the expanding gas until they are extracted from the expansion with a pulsed electric field.

As a result of the fact that the *ion–neutral* collision rate is independent of temperature, the ions remain reactively coupled to the neutral bath long after *neutral–neutral* collisions cease to be important. The internally excited cluster ions resulting from these ion–neutral association reactions are stabilized through collisions with neutral bath molecules during the lifetime of the metastable complex or through evaporative cooling. Cluster ions stabilized through collisions will equilibrate to the temperature of the expansion, which is on the order of 20–40 K.[118] Clusters ions that cool evaporatively retain enough internal energy to eject an additional monomer from the cluster ion; however, this occurs on a time scale much greater than the transit time through our spectrometer. Temperatures of these cluster ions are estimated through RRKM calculations to be ≈50–60 K.[32] Depending upon the relative contributions of collisional and evaporative cooling, the internal temperatures of the cluster ions will be on the order of 20–60 K.

When iodine vapor is seeded (≈1%) in the CO_2 supersonic expansion, the mass spectrum depicted in Figure 2 is observed. Two types of cluster ions are indicated in the figure: anionic

(119) Misaizu, F.; Mitsuke, K.; Kondow, T.; Kuchitsu, K. *J. Chem. Phys.* **1991**, *94*, 243.
(120) Gord, J. R.; Garrett, A. W.; Bandy, R. E.; Zwier, T. S. *Chem. Phys. Lett.* **1990**, *171*, 443.

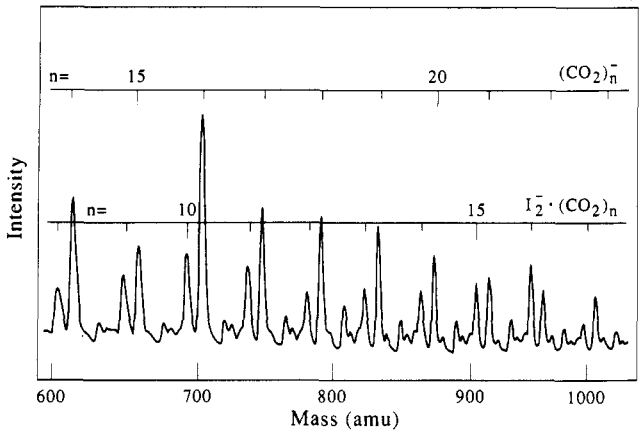

Figure 2. Negative ion mass spectrum observed with I_2 (≈1%) and CO_2 in the expansion. Both $I_2^-(CO_2)_n$ and $(CO_2)_n^-$ cluster ions are observed. Smaller unlabeled peaks correspond to $[H_2O(CO_2)_n]^-$ cluster ions. A sharp intensity drop is observed between $I_2^-(CO_2)_{16}$ and $I_2^-(CO_2)_{17}$.

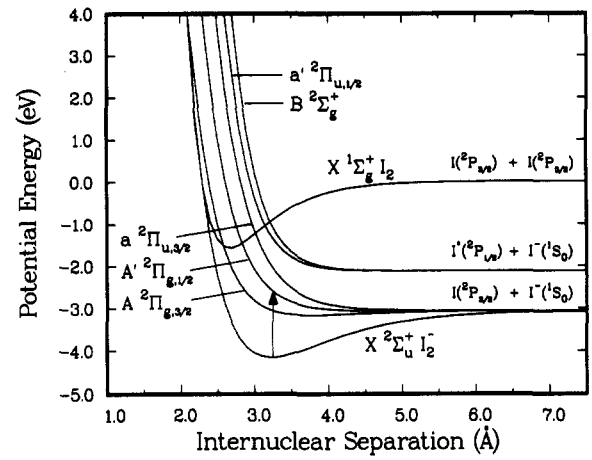

Figure 3. Potential energy curves for I_2^- as determined by Chen and Wentworth (ref 27). The arrow indicates the A' $^2\Pi_{g,1/2} \leftarrow$ X $^2\Sigma_u^+$ near-infrared transition excited by using a 720-nm photon. The ground-state potential energy curve for I_2 is included for comparison.

clusters of the neat CO_2 carrier gas, $(CO_2)_n^-$, and the $I_2^-(CO_2)_n$ cluster ion progression. Smaller unlabeled peaks correspond to $[H_2O(CO_2)_n]^-$ cluster ions arising from traces of water in the gas handling system. While only a small segment of the mass spectrum is displayed in the figure, $(CO_2)_n^-$ cluster ions to n = 60 and $I_2^-(CO_2)_n$ cluster ions to n = 55 are readily produced. There are a number of noteworthy features in the observed mass spectrum. First, an intensity anomaly indicative of a particularly stable cluster ion (magic number) is observed in the neat $(CO_2)_n^-$ cluster ion series at n = 16, as previously described.[118,121] Similar anomalies are also evident in the $I_2^-(CO_2)_n$ cluster ions. The $I_2^-(CO_2)_n$ intensity drops significantly (by approximately a factor of 4) after n = 16 and remains relatively constant for $n \geq 17$. A similar discontinuous drop in intensity occurs in the mass spectrum of $Br_2^-(CO_2)_n$ cluster ions;[31] however, in the bromine case this anomaly occurs at n = 12 rather than n = 16. Often this type of magic number behavior is associated with the formation of particularly stable species, such as those observed at electronic shell closings in clusters and their ions[122] or upon the closing of icosohedral shells in rare-gas cluster ions.[123-126] Recent MD simulations[115] and the photofragmentation data presented here suggest that these intensity variations are due to completion of the first solvation sphere around the anionic dihalogen. The solvation sphere around I_2^- is expected to be larger than that around Br_2^-, consistent with the n dependence of the observed anomalies.

B. Nanosecond Photoabsorption and Photofragmentation Experiments. Photophysical studies of $I_2^-(CO_2)_n$ cluster ions were performed to investigate the electronic structure of the parent ions and to identify trends in the photodissociation product ions. The results of the nanosecond photoabsorption studies demonstrate that the I_2^- visible photoabsorption band remains intact across the precursor cluster ion size range studied. We probed the effects of stepwise solvation on the photodissociation and subsequent recombination dynamics of I_2^- in mass-selected $I_2^-(CO_2)_n$. These experiments reveal that both I^-- and I_2^--based photofragment ions are produced upon photoexcitation of I_2^- in the cluster ion to a dissociative electronic state. Simple energetic arguments indicate that dissociated I_2^- recombines and vibrationally relaxes following absorption of a near-infrared photon to form the I_2^--based photofragment ions. Finally, these studies show that the quantum yield for recombination is strongly dependent on cluster ion size.

Photodestruction Cross-Section Measurements. The effects of solvation on I_2^- can be evaluated by measuring the photoabsorption spectrum for I_2^- and determining how the wavelength-resolved cross section changes with increasing cluster ion size. However, rather than evaluate the full photoabsorption spectrum for each cluster ion, we can investigate the size effects by measuring the absolute cross section for each cluster ion at a fixed wavelength. Any solvent shift in the photoabsorption cross section with increasing size will be reflected in a change in the absolute cross section at that fixed wavelength. Sensitive measurement of the relative cross section at a series of wavelengths is achieved by monitoring the appearance of neutral photofragments. Absolute cross sections are determined by measuring the *photodepletion* of the parent cluster ion signal.

Gas-phase potential energy curves for I_2^- computed by Chen and Wentworth[127] based on experimental data are displayed in Figure 3. To establish the identity of the chromophore in the $I_2^-(CO_2)_n$ cluster ions, we measured the photodestruction spectrum of I_2^-, which is depicted in Figure 4. The relative cross sections were obtained by monitoring the appearance of I on the in-line detector following the photodissociation of I_2^-. This neutral I signal was normalized to the parent I_2^- intensity measured on the off-axis detector and to fluctuations in laser intensity as previously described.[128,129] The photodestruction spectrum spans three dye curves, and measurements performed with a given dye were scaled to the others based on cross sections determined in overlapping regions of the dye curves. The entire spectrum was scaled to the absolute photodestruction cross section at 720 nm (vide infra) as determined by parent ion depletion.[128,129] The error limits displayed represent statistical fluctuations in the relative measurements as well as statistical error in the absolute cross section used to scale the spectrum (one standard deviation on the mean).

The observed photodestruction band is ≈1500 cm^{-1} wide (fwhm) and peaks around 750 nm. This spectrum is in good agreement with the A' $^2\Pi_{g,1/2} \leftarrow$ X $^2\Sigma_u^+$ transition recorded for I_2^- in solid KI by Delbecq et al.[130] The band that they observed is ≈1600 cm^{-1} wide (fwhm) and peaks at ≈800 nm.

Ideally, we could record full photodestruction spectra for all cluster ion sizes of interest; however, the effort required to obtain these full cross sections is prohibitive. Rather, we measured the full cross section for I_2^- and looked at the larger cluster ions at a selected wavelength. The spectrum in Figure 4 indicates that the derivative of the I_2^- wavelength-dependent cross section is

(121) Alexander, M. L.; Johnson, M. A.; Levinger, N. E.; Lineberger, W. C. *Phys. Rev. Lett.* **1986**, *57*, 976.
(122) Cohen, M. L.; Knight, W. D. *Phys. Today* **1990**, *43*, 42.
(123) Miehle, W.; Kandler, O.; Leisner, T.; Echt, O. *J. Chem. Phys.* **1989**, *91*, 5940.
(124) Echt, O.; Cook, M. C.; Castleman, A. W. Jr. *Chem. Phys. Lett.* **1987**, *135*, 229.
(125) Märk, T. D.; Scheier, P.; Leiter, K.; Ritter, W.; Stephan, K.; Stamatovic, A. *Int. J. Mass Spectrom. Ion Processes* **1986**, *74*, 281.
(126) Haberland, H. In *Electronic and Atomic Collisions*; Eichler, J., Hertel, I. V., Stolterfoht, N., Eds.; North-Holland: New York, 1984; p 597.
(127) Chen, E. C. M.; Wentworth, W. E. *J. Phys. Chem.* **1985**, *89*, 4099.
(128) Levinger, N. E.; Ray, D.; Alexander, M. L.; Lineberger, W. C. *J. Chem. Phys.* **1988**, *89*, 5654.
(129) Levinger, N. E.; Ray, D.; Murray, K. K.; Mullin, A. S.; Schulz, C. P.; Lineberger, W. C. *J. Chem. Phys.* **1988**, *89*, 71.
(130) Delbecq, C. J.; Hayes, W.; Yuster, P. H. *Phys. Rev.* **1961**, *121*, 1043.

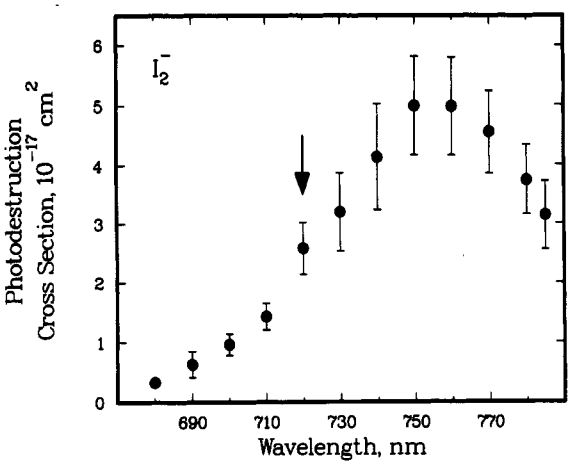

Figure 4. Absolute I_2^- photodestruction cross section. The error limits represent one standard deviation statistical fluctuation on the mean. The uncertainty in the absolute cross section is a factor of 2. The vertical arrow indicates the wavelength (720 nm) at which cross-section measurements for $I_2^-(CO_2)_n$ cluster ions were performed. See text for details.

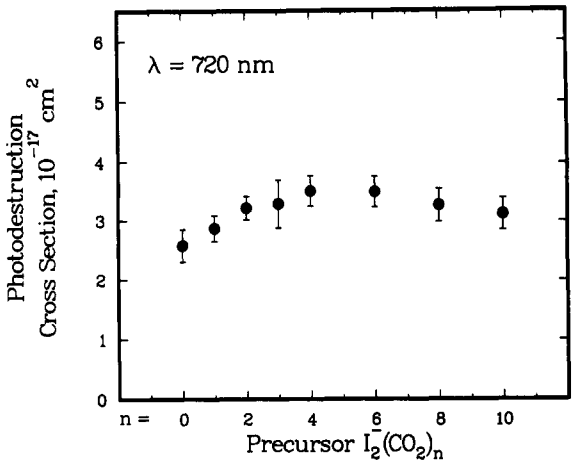

Figure 5. Absolute $I_2^-(CO_2)_n$ photodestruction cross sections at 720 nm. The error limits represent one standard deviation statistical fluctuation on the mean. The uncertainty in the overall absolute cross section is a factor of 2.

maximized at 720 nm, making this a sensitive wavelength to spectral shifts. If the photodestruction spectrum of the $I_2^-(CO_2)_n$ cluster ions were to shift toward the blue with increasing n, an increase in the cross section at 720 nm would be observed. Alternatively, a spectral shift to the red with increasing n would lead to a decrease in the cross section at 720 nm. The arrow in Figure 3 indicates the $A'\,^2\Pi_{g,1/2} \leftarrow X\,^2\Sigma_u^+$ transition accessed with a 720-nm photon in these photophysical studies. The photodestruction cross section measured at 720 nm is displayed as a function of cluster ion size in Figure 5. These cross-section data were obtained by monitoring the depletion of the parent cluster ion signal at the off-axis detector and normalizing to the laser intensity.[128,129] Cross sections were extracted based on the Beer–Lambert law. This approach to determining photodestruction cross sections eliminates any mass-dependent detection efficiency of the particle multiplier; therefore, good relative measurements are obtained. In principle, this appraoch also provides absolute cross sections; however, it is rather sensitive to systematic effects, such as spatial inhomogeneity of the laser, and the *absolute* cross-section measurement has an uncertainty of approximately a factor of 2. More careful detailed measurements could reduce this systematic error but have not been attempted in this work. Once again, the error limits in Figure 5 are one standard deviation on the mean and reflect only the statistical error in the measurement.

Figure 5 clearly demonstrates that the cross section at 720 nm does not change significantly with increasing solvation. This suggests that I_2^- remains the cluster ion chromophore across the size range studied and that the CO_2 solvent molecules do not significantly perturb its electronic structure in this spectral region. The fact that CO_2^- is not a stable anion ($EA(CO_2) = -0.6$ eV)[131] further supports our contention that the electronic structure of the cluster ions is similar to that of I_2^- and that significant delocalization of the charge onto surrounding CO_2 molecules does not occur. This result is confirmed by the matrix studies of Delbecq et al.[130] However, recent photoelectron spectra of $I^-{\cdot}CO_2$ show excitation of the CO_2 bend motion,[132] implying some charge delocalization from I^- onto CO_2 in the complex.

Photofragmentation Data at 720 nm. Interaction of the mass-selected ion beam with a 720-nm laser pulse results in the production of two types of photofragment ions, I^-- and I_2^--based:

$$I_2^-(CO_2)_n + h\nu \rightarrow I^-(CO_2)_m + I + (n-m)CO_2 \quad (3.1)$$

$$I_2^-(CO_2)_n + h\nu \rightarrow I_2^-(CO_2)_k + (n-k)CO_2 \quad (3.2)$$

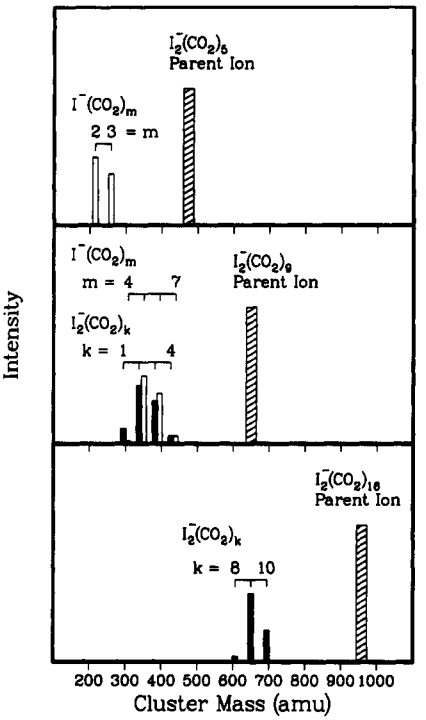

Figure 6. Photofragmentation mass spectra for representative precursor ions: $I_2^-(CO_2)_5$, $I_2^-(CO_2)_9$, and $I_2^-(CO_2)_{16}$. The low mass distribution represents the photofragments observed following the absorption of a 720-nm photon. The relative intensities of the photofragment ions are drawn to scale; however, the intensity of the precursor ion is not. Cross-hatched bars represent parent ions, open bars represent uncaged photofragment ions, and filled bars represent caged photofragment ions.

These fragment ions are observed at the off-axis detector ≈ 10 μs after laser excitation, and there is no evidence for dissociation in the reflectron. Photofragment ion distributions were obtained for $1 \leq n \leq 22$; those for $n = 5$, 9, and 16 are shown in Figure 6. These data are representative of three regions of size dependence observed in the branching ratio between reactions 3.1 and 3.2. The photofragmentation spectrum of $I_2^-(CO_2)_5$ exhibits only I^--based fragment ions, while $I_2^-(CO_2)_{16}$ photofragments to produce only I_2^--based fragment ions. In fact, for $n \leq 5$ only I^--based photofragments are observed, and for $n \geq 16$ only I_2^--based photofragments are observed. $I_2^-(CO_2)_9$ is representative of the transition region $6 \leq n \leq 15$, in which both types of photofragments are produced.

Simple energetic arguments applied to the I_2^--based photofragment ions indicate that recombination and vibrational relaxation of the photodissociated I_2^- chromophore have occurred.

(131) Compton, R. N.; Reinhardt, P. W.; Cooper, C. D. *J. Chem. Phys.* **1975**, *63*, 3821.

(132) Neumark, D. M. Presented at the 199th ACS National Meeting, Miami, FL, Sept 1989.

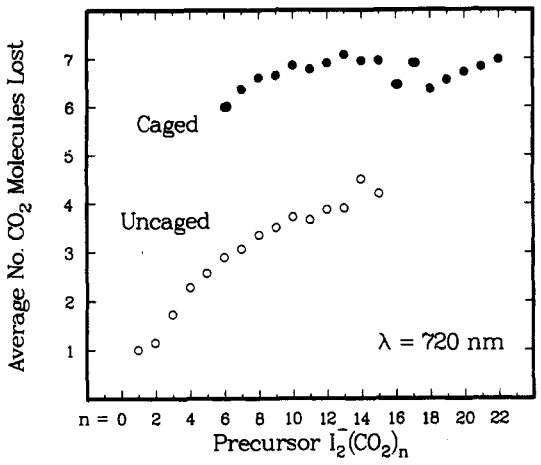

Figure 7. Average number of CO_2 molecules lost to form caged and uncaged photofragment ions following the absorption of a 720-nm photon.

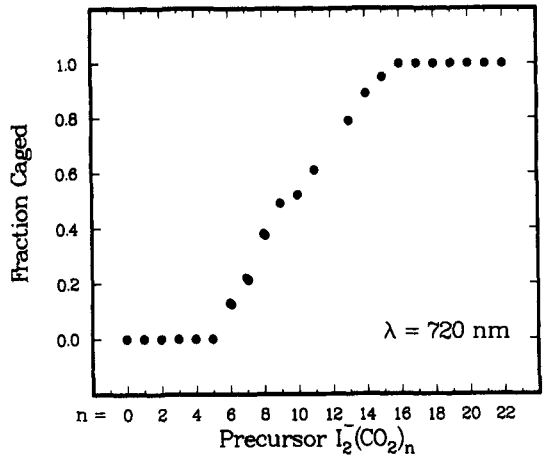

Figure 8. Branching ratio for the production of caged photofragment ions as a function of precursor cluster ion size following absorption of a 720-nm photon.

Determination of the average number of CO_2 molecules lost through evaporation in the large cluster ion limit permits the calculation of the CO_2 binding energy. The average number of CO_2 molecules ejected as a function of cluster ion size for the I^-- and I_2^--based photofragments is displayed in Figure 7. The number ejected during the production of I_2^--based photofragment ions is on the order of seven CO_2 molecules for $10 \leq n \leq 22$. If photodissociated I_2^- recombines and completely vibrationally relaxes in the I_2^--based photofragment ions, then all of the photon energy deposited in the cluster ion contributes to the evaporation of CO_2 molecules. Under these conditions, a binding energy can be determined from the photon energy and the average number of CO_2 molecules lost following photoexcitation.

Earlier experiments on $(CO_2)_n^+$ and $(CO_2)_n^-$ cluster ions indicate that CO_2 binding energies are ≈200 meV independent of the ionic core.[121,133] Of course, the CO_2 binding energy derived in this manner includes not only the energy required to remove a CO_2 molecule from the cluster ion but also any kinetic energy partitioned to the CO_2 molecule during evaporation. An RRKM analysis performed by Engelking[134] predicts a CO_2 binding energy of ≈150 meV and ascribes the difference between this value and our experimental "binding" energy to kinetic excitation of departing CO_2 molecules. Calculation of "binding" energies in this manner further assumes that the residual energy in the photofragment ion after CO_2 evaporation is nearly equal to the internal energy of the precursor cluster ion prior to photoexcitation. On the basis of RRKM calculations for Ar_n^+ cluster ions,[32] we expect that $I_2^-(CO_2)_n$ cluster ions will have about one bond energy of internal excitation prior to photoabsorption. If the initial internal energies are larger than this, the rate for unimolecular dissociation will increase substantially, leading to CO_2 evaporation during the time between cluster ion extraction and photoexcitation (≈100 μs). After photoexcitation, rapid evaporation of CO_2 molecules will occur until the internal energy is small enough that the time for unimolecular dissociation becomes greater than the flight time from the laser interaction region to the entrance of the reflectron (≈5 μs). The RRKM calculations suggest that on these time scales the cluster ions contain up to approximately one bond energy of internal excitation both before photoexcitation and after photofragmentation.

On the basis of the binding energy determined for the neat CO_2 cluster ions and the photofragmentation behavior observed for $Br_2^-(CO_2)_n$ cluster ions,[31] we expect that the average number of CO_2 molecules lost in $I_2^-(CO_2)_n$ cluster ions after absorption of a 720-nm photon will eventually reach an asymptotic value of ≈8.4 for large n. The observed loss of seven CO_2 molecules for $10 \leq n \leq 22$ indicates that most of the photon energy is converted into CO_2 evaporation and shows that the photodissociated I_2^- must have recombined and transferred much of its vibrational energy to the CO_2 solvent in the I_2^--based photofragment ions. Since the bond energy of I_2^-, ≈1 eV,[127] is not recovered in the I^--based photofragment ions, the number of CO_2 molecules lost is appropriately smaller. In the small cluster limit, the size of the fragment ions produced by photodissociation is particularly sensitive to the parent cluster ion geometry and CO_2 binding energies, which are likely to vary with cluster ion size and fragment ionic core; therefore, these calorimetric arguments are best applied to larger cluster ions in which the number of CO_2 molecules lost should reach an asymptotic value.

Since the I_2^--based photofragments contain recombined I_2^-, we can accurately describe them as "caged" photoproducts, indicating that the CO_2 solvent cage currounding the I_2^- chromophore induces recombination of I and I^-. Then we can define a quantum yield for caging or "caging fraction", which is simply the branching ratio for production of caged photoproducts as given in reaction 3.2. Figure 8 shows this caging fraction as a function of cluster ion size. The three regions noted above are clearly represented. For $n \leq 5$ the caging quantum yield is zero, for $n \geq 16$ it is unity, and it increases smoothly across the transition region $6 \leq n \leq 15$. The onset of complete caging at $I_2^-(CO_2)_{16}$, in conjunction with the mass spectral intensity anomaly at this cluster ion size, supports the contention that the first solvation shell closes at $n = 16$. Comparisons of the size-dependent caging fraction in $I_2^-(CO_2)_n$ cluster ions with the data collected for $Br_2^-(CO_2)_n$[31] show that closing of the Br^--based photofragment channel coincides with the magic number observed in the mass spectrum at $n = 12$, suggesting, once again, that 12 CO_2 molecules are contained in the first solvation shell around Br_2^-.

When $I_2^-(CO_2)_n$ photofragmentation experiments are performed at much higher laser power (<1.5 MW/cm², 6-ns pulse), a second group of fragment ions is observed at lower mass, well separated from the one-photon fragment ion distribution. Figure 9 illustrates the effects of low and high laser power on the distribution of fragment ions produced by photoexcitation of $I_2^-(CO_2)_{16}$. Based on the CO_2 binding energy calculated above and the number of CO_2 molecules ejected, the lower mass ions formed under high-power conditions are two-photon photofragments. The intensity of these low-mass photoproducts is quadratically dependent on laser power. The one- and two-photon fragment ion distributions for all caged precursor ions are qualitatively similar, with widths on the order of two to three CO_2 masses. The most prominent one- and two-photon photofragment ions produced for precursors with $9 \leq n \leq 16$ are listed in Table I.

In summary, these nanosecond laser experiments indicate that I_2^- is the near-infrared chromophore in these $I_2^-(CO_2)_n$ cluster ions and that this transition is essentially unaffected with increasing cluster ion size. Simple energetic arguments applied to the observed photofragment distributions reveal that the CO_2 solvent

(133) Alexander, M. L.; Johnson, M. A.; Lineberger, W. C. *J. Chem. Phys.* **1985**, *82*, 5288.
(134) Engelking, P. C. *J. Chem. Phys.* **1986**, *85*, 3103.

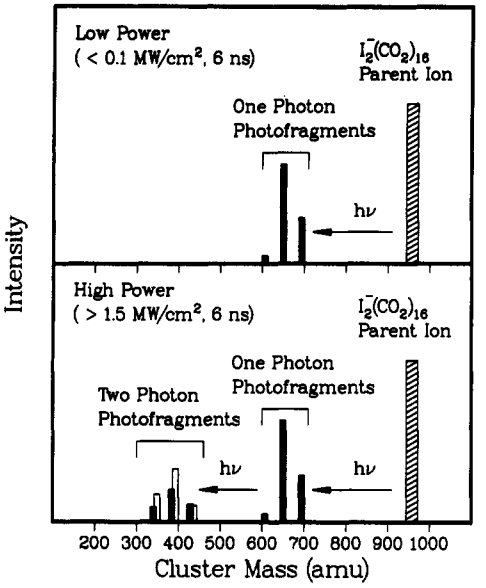

Figure 9. Effects of laser power on the photofragment ion distribution for $I_2^-(CO_2)_{16}$. At low laser powers, only one-photon photofragment ions are observed, while at higher laser powers, both one- and two-photon photofragment ions are observed as shown. Cross-hatched bars represent parent ions, open bars represent uncaged photofragment ions, and filled bars represent caged photofragment ions.

TABLE I: Summary of the One- and Two-Photon Photofragment Ion Distributions from $I_2^-(CO_2)_n$ Cluster Ions following 720-nm Excitation

precursor cluster ion $I_2^-(CO_2)_n$, n =	one-photon photofragment ion[a] $I_2^-(CO_2)_k$, k =	two-photon photofragment ion[b] $I^-(CO_2)_l$, l =
9	2	1
10	3	1
11	4	2
13	6	3
14	7	4
15	8	5
16	9	6

[a] Most probable caged one-photon photofragment ion. This fragment ion is typically near the center of the photofragment ion distribution, which is two to three CO_2 monomers wide. The most probable photofragment ion is within half a monomer unit of the mean of the distribution. [b] Most probable two-photon photofragment ion. This fragment ion is typically near the center of the photofragment ion distribution, which is ≤3 CO_2 monomers wide. The most probable photofragment ion is within half a monomer unit of the mean of the distribution.

molecules can cage the photodissociated I_2^- chromophore and that the quantum yield for this caging process is strongly cluster ion size dependent. Finally, photodissociation products corresponding to the absorption of two photons can be observed at high laser power. These static experiments set the stage for pump–probe studies of the recombination dynamics described in the following section.

C. Time-Resolved Picosecond Dynamics. The existence of the two-photon photofragment ion distribution suggests that these photoproducts can be used to monitor time-resolved recombination dynamics in size-selected $I_2^-(CO_2)_n$ cluster ions via pump–probe techniques. A schematic representation of such a pump–probe experiment is presented in Figure 10. A picosecond pump pulse excites I_2^- to the repulsive $A'\,^2\Pi_{g,1/2}$ excited state where it then dissociates. If the CO_2 solvent cage is sufficiently developed, it can induce recombination of the dissociating chromophore, producing I_2^- in a highly excited vibrational level of the ground electronic state. Once the recombined I_2^- has lost ≈75% of its vibrational energy, it can absorb a second photon of the same color, this time from a probe pulse, resulting in the formation of two-photon fragment ions such as those observed under high-power conditions in the nanosecond experiments. The intensity of these

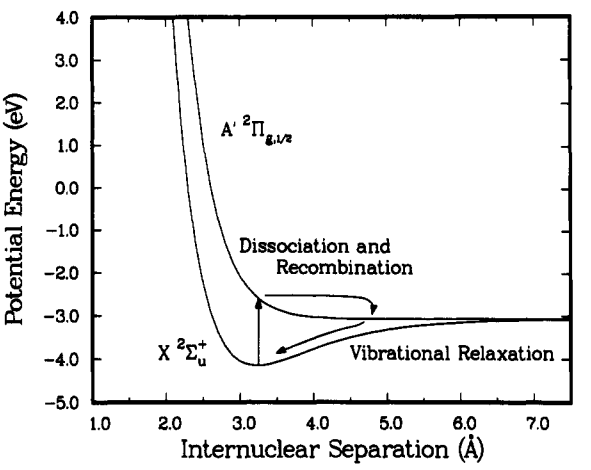

Figure 10. Schematic representation of the sequential two-photon absorption mechanism. After absorption of the first photon, the CO_2 cluster can induce recombination of the dissociating I_2^- onto the ground-state potential energy curves. The resulting highly vibrationally excited I_2^- partially relaxes after which it can absorb a second photon.

two-photon product ions measured as a function of delay between the pump and probe pulses maps out a transient bleaching curve. Furthermore, the intensity of the two-photon product ions generated from a *single* laser pulse will depend sensitively on the absorption recovery time if the laser pulse duration is comparable to the time scale for recombination and vibrational relaxation. Under these conditions, a single laser pulse could be used to investigate the evolution of size effects on the photodissociation/geminate recombination dynamics in $I_2^-(CO_2)_n$ cluster ions. These two experiments are described in detail below.

Time-Resolved Pump–Probe Experiments. Observation of a transient bleach in the two-photon photofragment ion intensity requires that the *sequential* absorption of two photons dominates over any coherent two-photon absorption process. Furthermore, a simple interpretation of the bleaching signal will be possible only if I_2^- is the only chromophore in these cluster ions at 720 nm and if the absorption cross section is independent of cluster ion size. Following I_2^- photodissociation, I, I^-, $I^-(CO_2)_m$, CO_2, and $(CO_2)_n^-$ could be present in the photoexcited cluster ion. If any of these species were to carry oscillator strength at 720 nm, absorption of a second photon could occur independent of I_2^- recombination. The recorded spectra of I[135] and CO_2[136] show no absorption at 720 nm. I^- supports no bound excited electronic states and is transparent at 720 nm. Photodestruction spectra of $(CO_2)_n^-$[121] and $I^-(CO_2)_n$ cluster ions have been measured, and these species do not exhibit detectable photoproduct ions following irradiation at 720 nm. Thus, I_2^- remains the only important chromophore at 720 nm. If the photoabsorption cross section were to change with cluster ion size, then a photoexcited ion's propensity to absorb a second photon would change as it evaporatively cooled. Under these conditions, a transient signal due to the evaporation process would be superimposed on the transient response due to I_2^- recombination. However, our data demonstrate that the photodestruction cross section are relatively independent of cluster ion size at 720 nm (Figure 5).

Transient bleaching curves are displayed in Figure 11 for $I_2^-(CO_2)_9$ and $I_2^-(CO_2)_{16}$. This transient bleaching signal was obtained by normalizing the count rate of the two-photon fragment ions to the count rate obtained for the one-photon fragment ions as a function of delay between pump and probe pulses. The curves drawn through the data are single-exponential recoveries, $[1 - \exp(-|t|/\tau)]$, convoluted with a Gaussian instrument response function (6 ps fwhm), which is due primarily to counterpropagation of the pump and probe pulses. The recovery time, τ, is 30 ± 10 ps for $I_2^-(CO_2)_9$ and 10 ± 5 ps for $I_2^-(CO_2)_{16}$.[42] Since both the

(135) Moore, C. E. *Circ.—Natl. Bur. Stand. (U.S.)* **467** 1957, *3*, 105.
(136) Herzberg, G. *Electronic Spectra of Polyatomic Molecules*; Van Nostrand: Princeton, 1966.

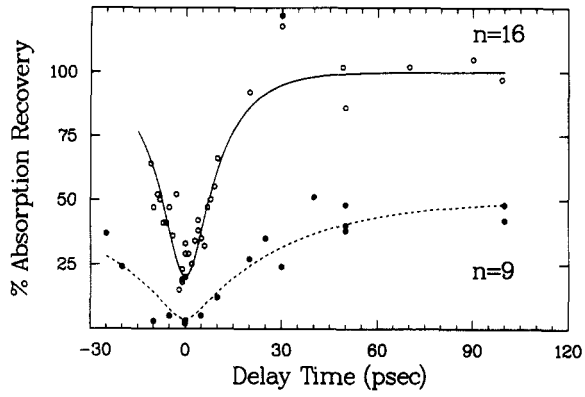

Figure 11. Transient bleaching data for $I_2^-(CO_2)_{16}$ (filled circles) and $I_2^-(CO_2)_9$ (open circles) at 720 nm measured by using picosecond pump–probe techniques. The solid and dashed lines are single-exponential recoveries convoluted with the ≈6-ps instrument response. Recovery times, τ, are 30 ± 10 ps for $I_2^-(CO_2)_9$ and 10 ± 5 ps for $I_2^-(CO_2)_{16}$. (Reproduced with permission from ref 42. Copyright 1989 American Institute of Physics.)

pump and probe laser pulses are identical in all respects, the transient bleaching curves are symmetric about zero delay.

If coherent two-photon absorption were an important process in these cluster ions, then we would expect to see a significant signal with zero pump–probe delay. In fact, the small absorption recovery observed at short delay times can be totally accounted for by the instrument response function. These transient bleaching results confirm that two-photon photofragment ions are generated from precursor cluster ions through a *sequential* absorption mechanism. The scatter in the data justifies only a simple model of this sequential mechanism:

$$I_2^-(CO_2)_n + h\nu \xrightarrow{\sigma_n F_n} I_2^-(CO_2)_k + h\nu \xrightarrow{\sigma_k[1-\exp(-|t|/\tau)]} I_2^-(CO_2)_j$$

$$\sigma_n(1-F_n) \rightarrow I^-(CO_2)_m \qquad I^-(CO_2)_l$$

one-photon products; two-photon products

(3.3)

In (3.3), σ is the photoabsorption cross section at 720 nm, and F_n is the caging fraction for a given parent cluster ion at this wavelength. The characteristic time for recovery of the absorption cross section is τ. In order to turn τ into physically meaningful populations, it is necessary to know the absorption cross section for $I_2^-(CO_2)_n$ as a function of n, the degree of internal excitation of the cluster ion, and the amount of vibrational excitation in the I_2^- bond. The nanosecond experiments described above indicate that the absorption cross section is relatively independent of the number of CO_2 molecules in the cluster ion, i.e. $\sigma_n \approx \sigma_k$. This observation also supports the notion that the absorption cross section for a given I_2^- vibrational energy is not strongly affected by excess energy in the CO_2 solvent degrees of freedom. Thus, the issue of the absorption recovery centers on the cross section, σ_k, as a function of the I_2^- vibrational energy content. Based upon inspection of Figure 3, the absorption cross section regains most of its intensity when recombined I_2^- has given up ≈75% of its initial vibrational energy to the CO_2 bath. Collectively, these observations and assumptions imply that the recovery time, τ, can be viewed physically as the time constant for the dissociated I_2^- to recombine and vibrationally relax.

The branching ratio between formation of I^-- and I_2^--based photofragment ions after absorption of a single photon by $I_2^-(CO_2)_n$ is dictated by the caging fraction, F_n. The partitioning of the two-photon products between I^-- and I_2^--based photofragment ions is controlled by the various caging fractions of the one-photon fragment ions, $I_2^-(CO_2)_k$. The second photon is absorbed only after photodissociated I_2^- recombines and transfers much of its vibrational energy to the CO_2 solvent, which occurs tens of picoseconds after absorption of the first photon. However, evaporation is incomplete on this time scale, so the cluster ion which absorbs the second photon is internally excited. Hence, the caging fractions measured for the relatively cold parent cluster ions may not provide an accurate description of the caging fractions for the nascent $I_2^-(CO_2)_k$.

The number of $I_2^-(CO_2)_k$ one-photon fragment ions that are capable of absorbing a second photon of the same color changes with time as the photodissociated I_2^- recombines on the ground-state surface and vibrationally relaxes. This time dependence is included in (3.3) through the exponential absorption recovery suggested by the results of the pump–probe experiments. Uncaged cluster ions, $I^-(CO_2)_m$, will never be able to absorb another 720-nm photon, resulting in a permanent loss in the absorption recovery; therefore, the asymptotic limits approach the caging fraction at very long delay times ($\gg\tau$). (See Figure 11.)

The observation of a transient bleach in this experiment demonstrates that a sequential two-photon absorption process occurs in these $I_2^-(CO_2)_n$ cluster ions. The time scale for absorption recovery is on the order of tens of picoseconds and is cluster ion size dependent. A knowledge of these size-dependent recovery times for cluster ions between $I_2^-(CO_2)_9$ and $I_2^-(CO_2)_{16}$ could provide some insight into the contributions of dissociation/recombination and vibrational relaxation to the absorption recovery.

Time-Resolved Single-Pulse Experiments. Our principal goal is elucidation of the effects of stepwise solvation on the photodissociation/geminate recombination dynamics. While substantial dynamical information is contained in transient bleaching curves such as those displayed in Figure 11, the experiments designed to collect these data are both complex and time-consuming. The results of the picosecond pump–probe experiments suggest that the absorption recovery times for $I_2^-(CO_2)_n$ cluster ions in the size range $9 \le n \le 16$ are on the order of 20 ps. Therefore, the number of two-photon product ions generated in a single pulse of this duration should be a sensitive indicator of the absorption recovery time for cluster ions in this size range. Measurement of this two-photon signal permits us to survey the evolution of size effects in the absorption recovery times. Furthermore, the level of complexity and the time required to perform the single-pulse experiment are significantly reduced with respect to the pump–probe studies, so that many cluster ion sizes can be rapidly investigated.

The number of two-photon photofragment ions produced in a single laser pulse depends on the duration of the laser pulse and the time scale for absorption recovery. For a single laser pulse with width much greater than τ, many two-photon product ions will be generated, but the number observed will be insensitive to changes in the absorption recovery time. At the other temporal extreme, a single laser pulse of the same pulse energy, but with duration much shorter than τ, produces essentially no two-photon product ions. However, the number of two-photon product ions formed in a single laser pulse whose duration is comparable to τ will be measurable and dependent on the time scale for absorption recovery. This is the situation observed in the pump–probe experiment when two counterpropagated picosecond pulses are overlapped with a nominal delay time of zero (6 ps fwhm instrument response function). As seen in Figure 11, the number of two-photon product ions at zero delay is considerably larger for $I_2^-(CO_2)_{16}$ ($\tau \approx 10$ ps) than for $I_2^-(CO_2)_9$ ($\tau \approx 30$ ps). Measurement of the number of two-photon fragment ions produced by a single laser pulse of fixed width can give qualitative cluster ion size dependent trends in absorption recovery time scales.

To quantify the dependence of the two-photon product ion yield on cluster ion size, we can define an apparent two-photon cross section:

$$\sigma_{2h\nu} = \frac{N_{2h\nu}}{FN_P\Phi^2}G = \frac{N'_{2h\nu}}{N'_P\Phi^2}\left(\frac{D_P}{FD_{2h\nu}}\right)G \qquad (3.4)$$

In this expression, $\sigma_{2h\nu}$ is the apparent two-photon cross section, $N_{2h\nu}$ is the number of two-photon photofragment ions, N_P is the number of parent cluster ions, F is the caging fraction for those parent ions, Φ is the time-integrated photon flux (photons per unit area), and G includes a number of geometrical factors. The actual

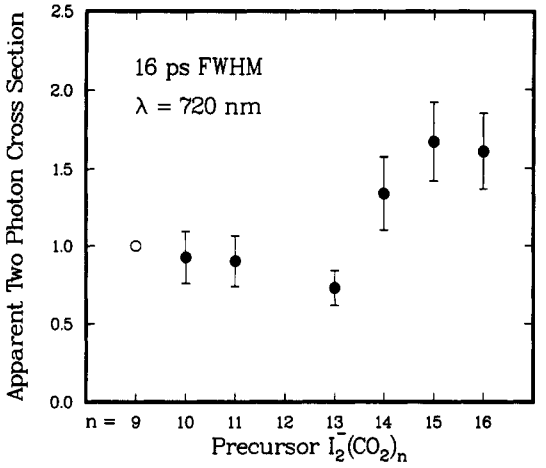

Figure 12. Apparent two-photon cross section as a function of precursor cluster ion size, obtained by using a single laser pulse (16 ps fwhm autocorrelation width) at 720 nm. All cross sections are relative to $I_2^-(CO_2)_9$.

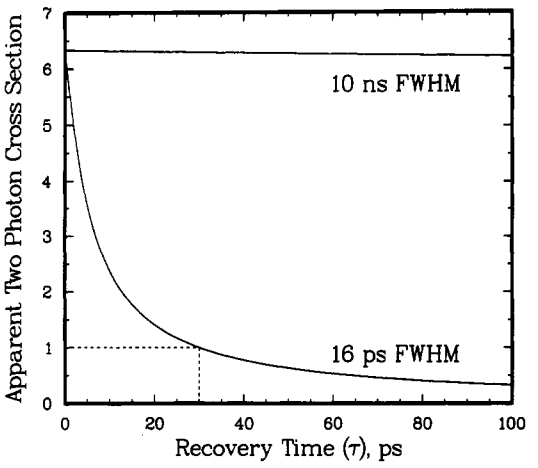

Figure 13. Apparent two-photon cross section as a function of absorption recovery time, τ, obtained from the model in eq 3.6 for 10-ns and 16-ps pulses (fwhm). The curves are scaled so that the apparent two-photon cross section for the 16-ps pulse is unity at an absorption recovery time of 30 ps.

number of two-photon photofragment ions, $N_{2h\nu}$, and the actual number of parent cluster ions, N_P, cannot be determined experimentally without some knowledge of the detection efficiencies of the particle multipliers, $D_{2h\nu}$ and D_P. Studies suggest that the detection efficiency of a channel electron multiplier depends on the velocity of the incident particle;[137] therefore, the signals observed on our particle multipliers will depend on cluster ion size. We designate the *measured* number of two-photon product ions and parent cluster ions as $N'_{2h\nu}$ and N'_P, respectively.

The caging fraction is included in the two-photon cross section to account for the fact that only caged one-photon photofragment ions can produce two-photon product ions. Instrumental geometry factors such as ion beam–laser overlap and homogeneity of the laser beam profile are included in G. Across the $9 \le n \le 16$ size range any differences in ion trajectories are small, so G is only weakly dependent on cluster ion size. Care was taken to ensure good laser beam quality and optimal overlap with the ions in an effort to minimize possible contributions to G.

The quantity determined experimentally in the single laser pulse experiment is $N'_{2h\nu}/N'_P\Phi^2$, which differs from $\sigma_{2h\nu}$ by the particle multiplier detection efficiencies, the caging fraction, and the geometrical factor. When a 6-ns laser pulse ($\gg\tau$) is employed, $\sigma_{2h\nu}$ is essentially independent of τ and is equal to its asymptotic limit, $\sigma^\infty_{2h\nu}$ ($\sigma^\infty_{2h\nu} = \sigma^2 \approx 6 \times 10^{-34}$ cm^4/cluster ion at 720 nm). With this long pulse excitation, the changes in $(N'_{2h\nu}/N'_P\Phi^2)_{ns}$ with cluster ion size reflect the n dependence of the particle multiplier detection efficiencies and the caging fraction. In essence, $(N'_{2h\nu}/N'_P\Phi^2)_{ns}$ determined with a 6-ns laser pulse is a direct experimental measurement of $\sigma^\infty_{2h\nu}(FD_{2h\nu}/GD_P)$.

However, $\sigma_{2h\nu}$ depends strongly on τ when the laser pulse width is on the order of the absorption recovery time (≈20 ps). In this case, $(N'_{2h\nu}/N'_P\Phi^2)_{ps}$ includes the changes in τ with cluster ion size, but it must be corrected for the n-dependent detection efficiencies and caging fraction in order to extract the changes in $\sigma_{2h\nu}$ with τ. This is accomplished by dividing $(N'_{2h\nu}/N'_P\Phi^2)_{ps}$ by $(N'_{2h\nu}/N'_P\Phi^2)_{ns}$. Since $(N'_{2h\nu}/N'_P\Phi^2)_{ns}$ is simply $\sigma^\infty_{2h\nu}(FD_{2h\nu}/GD_P)$, the ratio of $(N'_{2h\nu}/N'_P\Phi^2)_{ps}$ to $(N'_{2h\nu}/N'_P\Phi^2)_{ns}$ gives $\sigma_{2h\nu}/\sigma^\infty_{2h\nu}$. While an absolute measurement of the apparent two-photon cross section is possible, the values obtained relative to a particular cluster ion size are free from many of the systematic errors present in an absolute measurement. The apparent two-photon cross sections for cluster ions in the size range $9 \le n \le 16$ are displayed in Figure 12 relative to $I_2^-(CO_2)_9$. Faster absorption recovery will lead to more two-photon product ions and larger $\sigma_{2h\nu}$; therefore, the increase in apparent two-photon cross section for larger cluster ions indicates a decrease in the absorption recovery time. The data presented in Figure 12 suggest that a rapid change in τ occurs in the region $13 \le n \le 15$. We attempt to describe this rapid change more quantitatively by extracting τ values based on a model of the laser pulse and the absorption recovery.

A Gaussian function was used to describe the laser pulse, and the single exponential suggested in the pump–probe experiment, $[1 - \exp(-|t|/\tau)]$, was used to model the absorption recovery. Since the model is a function of the *delay* between absorption of the first and second photons, the number of two-photon product ions depends on the distribution of possible delay times contained in a single laser pulse. Furthermore, the apparent two-photon cross section observed from a single pulse is actually an average of the absorption recovery model over that distribution. That is

$$\sigma_{2h\nu} = \sigma^\infty_{2h\nu} \int_{-\infty}^{\infty} \left[1 - \exp\left(-\frac{|t|}{\tau}\right)\right] P(t)\, \mathrm{d}(t) \qquad (3.5)$$

where $P(t)$ is the distribution of possible delay times. The asymptotic apparent two-photon absorption cross section obtained with extremely large pulse widths ($\gg\tau$) is designated $\sigma^\infty_{2h\nu}$, as described above. For a Gaussian pulse, the distribution of possible delay times contained within that pulse is given by its autocorrelation function, which is also a Gaussian. The width of the autocorrelation function is related to the width of the laser pulse by $s_{ac} = \sqrt{2}s_{lp}$, where s_{ac} is the standard deviation of the autocorrelation function and s_{lp} is the standard deviation of the Gaussian function describing the laser pulse. With this in mind, evaluation of the integral in (3.5) gives

$$\sigma_{2h\nu}(\tau, s_{ac}) = \sigma^\infty_{2h\nu}\left[1 - \exp\left(\frac{{s_{ac}}^2}{2\tau^2}\right) \mathrm{erfc}\left(\frac{1}{\sqrt{2}}\frac{s_{ac}}{\tau}\right)\right] \qquad (3.6)$$

where erfc (x) is the complementary error function of x. Equation 3.6 illustrates both the recovery time and laser pulse width dependence of $\sigma_{2h\nu}$. For a given τ, this function is nearly zero for very short pulse widths ($\ll\tau$) and increases with increasing pulse width until it reaches its asymptotic limit, $\sigma^\infty_{2h\nu}$, for long pulses ($\gg\tau$). The autocorrelation function of our picosecond pulse is measured directly and has a fwhm of 16 ps. The corresponding quantity for the 6-ns laser pulse is ≈10 ns. The τ dependence of (3.6) for these two pulses is displayed in Figure 13. The curves are scaled so that the cross section determined with a 16-ps pulse is unity for an absorption recovery time of 30 ps. The apparent two-photon cross section is very sensitive to absorption recoveries on the order of 10–30 ps when a 16-ps pulse (fwhm autocorrelation width) is employed; however, a 6-ns laser pulse (≈10 ns fwhm delay time distribution) gives an essentially constant apparent two-photon cross section for recovery times less than 100 ps.

Since this experimental method only provides apparent two-photon cross sections *relative* to a particular cluster ion, the

(137) Campbell, E. E. B.; Ulmer, G.; Hasselberger, B.; Busmann, H.-G.; Hertel, I. V. *J. Chem. Phys.* **1990**, *93*, 6900.

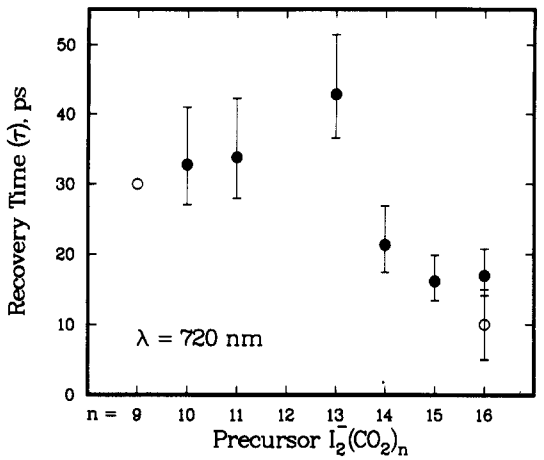

Figure 14. Absorption recovery times for $I_2^-(CO_2)_n$ in the size range $9 \leq n \leq 16$ at 720 nm. The recovery time for $I_2^-(CO_2)_9$ was fixed at 30 ps. Error limits for the other cluster ions were extracted from the model in eq 3.6 as described in the text. The absorption recovery time and associated error limits determined for $I_2^-(CO_2)_{16}$ (open circle) by using picosecond pump–probe techniques (ref 42) are included for comparison.

absorption recovery time for one of the cluster ions must be known in order to extract τ's from eq 3.6. Based on the pump–probe experiments, the recovery time for $I_2^-(CO_2)_9$ is 30 ± 10 ps.[42] The apparent cross sections in Figure 12 can be converted into recovery times based on $\tau = 30$ ps for $I_2^-(CO_2)_9$ by using eq 3.6. The resulting absorption recovery times are plotted in Figure 14.

The error limits displayed were obtained from the upper and lower limits of the relative cross-section data in Figure 12. The extraction process assumes that $\tau = 30$ ps for $I_2^-(CO_2)_9$, so no error limits are displayed for $n = 9$. Error limits on the remaining data represent the accuracy of the absorption recovery times relative to $I_2^-(CO_2)_9$. The absolute recovery times depend on the accuracy of the value determined for $n = 9$ in the transient bleaching experiment. Fixing the recovery time for $n = 9$ at 20 or 40 ps changes the absolute recovery times for the other cluster ions; however, the qualitative features remain the same. Also included in Figure 14 is the absorption recovery time and error limits measured for $I_2^-(CO_2)_{16}$ in the transient bleaching study. Overlapping of the error limits determined in the single-pulse and pump–probe experiments indicates that the two techniques give consistent results for this cluster ion.

It is important to note that the strength of the single-pulse technique lies in its ability to reveal qualitative trends in the size dependence of the absorption recovery time; however, it does not provide absolute measurements of τ. The most striking feature of these size-dependent absorption recovery times is that, rather than decreasing smoothly with increasing size, there appears to be a rapid change in τ over the cluster ion size range $13 \leq n \leq 15$. This rapid change is explored in simulations described in the next section.

D. Monte Carlo Simulations. Monte Carlo (MC) simulations employing the Metropolis algorithm[138] have been performed on $I_2^-(CO_2)_n$ ($n = 2$–9) to determine minimum-energy structures and equilibrium properties for these systems.

Details of the Simulation. The potential model employed in these calculations is the sum of three terms

$$V_{\text{total}} = \sum_{i<j} V_{i,j}(CO_2\text{–}CO_2) + \sum_i V_i(I_2^-\text{–}CO_2) + V_{\text{pol}} \quad (3.7)$$

where $V(CO_2\text{–}CO_2)$ is the CO_2–CO_2 pairwise interaction and $V(I_2^-\text{–}CO_2)$ is the I_2^-–CO_2 pairwise interaction. These are summed over all of the CO_2–CO_2 and I_2^-–CO_2 pairs. The last term, V_{pol}, is the collective polarization energy, which takes into account many-body effects in the formation of induced dipoles and their interaction with the static charges contained in the cluster ion.

The potential used to describe the CO_2–CO_2 interaction, $V(CO_2\text{–}CO_2)$, was developed by Murthy et al.[139] It describes each CO_2 molecule by three Lennard-Jones sites and five point charges placed inside the Lennard-Jones (LJ) hard spheres such that they reproduce the large quadrupole and three higher nonzero electrostatic moments of CO_2. Each LJ site interacts with LJ sites on other CO_2 molecules via the Lennard-Jones (6–12) potential. In addition, each point charge interacts with the point charges on the other CO_2 molecules via the Coulombic potential. Thus, the interaction energy for each CO_2–CO_2 pair is given by the sum of nine Lennard-Jones (6–12) terms and 25 Coulombic interactions. This potential reproduces the lattice vibrational frequencies of CO_2 solid[139] and the structure of CO_2 dimer.[140,141]

In the model used to describe the I_2^-–CO_2 interaction, $V(I_2^-\text{–}CO_2)$ is also written as the sum of Lennard-Jones (6–12) potential terms and Coulombic interactions between point charges. The CO_2 molecule is again described by three LJ sites and five point charges. The I_2^- is described by a LJ site and a $-e/2$ point charge located at the center of each iodine atom. Each LJ site on I_2^- interacts with the LJ sites on the CO_2 molecules via the Lennard-Jones (6–12) potential, while the point charges located at the center of each iodine atom interact with the point charges embedded in the CO_2 molecule via the Coulombic potential.

Determination of the polarization energy term involves a standard self-consistent-field (SCF) calculation of the induced dipoles.[113,142–144] Isotropic point polarizabilities are placed at the center of each CO_2 molecule and at the center of each iodine atom. After the induced dipoles are determined, the polarization energy is calculated as prescribed previously[145,146]

$$V_{\text{pol}} = -\tfrac{1}{2}\sum_i \vec{\mu}_i \cdot \vec{E}_i^{\circ} \quad (3.8)$$

where the sum is over all polarizable centers in the cluster, $\vec{\mu}_i$ is the induced dipole, and $\vec{E}_i^{\circ}$ is the electric field, due only to static charges, at the ith polarizable center. This model does not account for any delocalization of charge from the I_2^- onto the solvent CO_2 molecules[132] or extensive charge transfer within the I_2^- itself. Details are available from the authors upon request.

Initial configurations for the MC simulations were determined from the random placement of the CO_2 molecules around the I_2^- ion. Cluster ion annealing was performed in a manner similar to that employed by Lisy and co-workers.[147] Complete annealing of this randomly chosen configuration required the use of several "heat/cool" cycles. In each cycle the simulation was initiated at a temperature of 150 K, and 30 000 iterations per CO_2 were performed at this temperature. While the temperature was gradually reduced to 30 K, 10 000 additional iterations per CO_2 were carried out. Finally the temperature was held at 30 K for another 10 000 iterations per CO_2. During these final configurations, minimum-energy structures were observed. The relative root-mean-square bond length fluctuation, δ,[148–151] which is indicative of the mobility of a molecule within the cluster ion, was evaluated in a separate MC simulation at a variety of temperatures between 30 and 150 K. In these simulations, the minimum-energy structure was used as the initial configuration, and the system was equilibrated to the desired temperature before ensemble averages were determined.

(138) Metropolis, N.; Rosenbluth, A. W.; Rosenbluth, M. N.; Teller, A. H. *J. Chem. Phys.* **1953**, *21*, 1087.
(139) Murthy, C. S.; O'Shea, S. F.; McDonald, I. R. *Mol. Phys.* **1983**, *50*, 531.
(140) Walsh, M. A.; England, T. H.; Dyke, T. R.; Howard, B. J. *Chem. Phys. Lett.* **1987**, *142*, 265.
(141) Jucks, K. W.; Huang, Z. S.; Dayton, D.; Miller, R. E.; Lafferty, W. J. *J. Chem. Phys.* **1987**, *86*, 4341.
(142) Pollock, E. L.; Alder, B. J. *Phys. Rev. Lett.* **1987**, *41*, 903.
(143) Gay, J. G.; Berne, B. J. *Phys. Rev. Lett.* **1982**, *49*, 194.
(144) Stillinger, F. H.; David, C. W. *J. Chem. Phys.* **1978**, *69*, 1473.
(145) Cieplak, P.; Kollman, P. *J. Chem. Phys.* **1990**, *92*, 6761.
(146) Cieplak, P.; Kollman, P.; Lybrand, T. *J. Chem. Phys.* **1990**, *92*, 6755.
(147) Draves, J. A.; Luthey-Schulten, Z.; Liu, W.-L.; Lisy, J. M. *J. Chem. Phys.* **1990**, *93*, 4589.
(148) Davis, H. L.; Jellinek, J.; Berry, R. S. *J. Chem. Phys.* **1987**, *86*, 6456.
(149) Jellinek, J.; Beck, T. L.; Berry, R. S. *J. Chem. Phys.* **1986**, *84*, 2783.
(150) Beck, T. L.; Jellinek, J.; Berry, R. S. *Chem. Phys.* **1987**, *87*, 545.
(151) Etters, R. D.; Kaelberer, J. *J. Chem. Phys.* **1977**, *66*, 5112.

Results of the Simulation. We can draw several qualitative conclusions from the MC simulations. As described above, the three-term potential model gives rise to five interaction energies. In addition to the polarization energy, the $V(CO_2-CO_2)$ and $V(I_2^--CO_2)$ terms each include electrostatic interactions and LJ interactions. The first observation from the simulations is that the polarization and ion–quadrupole interactions make the largest contributions to the binding energy. As a result, I_2^- is clearly demonstrated to be embedded in the cluster surrounded by the CO_2 solvent shell, as opposed to occupying a surface site on a cluster of CO_2 molecules. This result agrees with the experimental observation of 100% caged photofragment ions for large cluster ions. Second, the minimum-energy structures reveal that clustering of CO_2 molecules begins around the I_2^- waist in a plane that is perpendicular to the internuclear axis. As more CO_2 molecules are added to the cluster, they are observed to "tip" in order to achieve favorable CO_2–CO_2 dimer bonding. Following the completion of a ring of CO_2 molecules around this waist, clustering continues around the iodine atoms themselves, and the CO_2 molecules begin to form a solvent cylinder coaxial with the I_2^- ion. Finally, evaluation of δ for ensembles equilibrated to temperatures characteristic of our experimental conditions (20–60 K) suggests that the cluster ions are fairly rigid.

Molecular dynamics (MD) simulations of these systems have been performed by Amar and Perera.[115] In their model they describe the electrostatic properties of CO_2 by using a point quadrupole; however, the remaining details of the MC and MD potential models are similar. Their MD results give minimum-energy structures that are consistent with ours. In addition, Amar and Perera have studied cluster ions to $n = 17$ and note several interesting features of these larger species. First, the cylinder of CO_2 molecules observed in the MC simulations continues to form with increasing n, and eventually "capped" structures are observed in which one or more CO_2 molecules occupy positions along the I_2^- internuclear axis. Second, the first solvation shell appears to close at $I_2^-(CO_2)_{16}$, which is consistent with the conclusions drawn from the mass spectral intensity anomaly and the caging fraction experimentally observed for this cluster ion.

E. Size Effects in the Absorption Recovery Time. The transient bleaching signal displayed in Figure 11 and the plot of absorption recovery times vs cluster ion size in Figure 14 indicate the existence of absorption recoveries which are strongly dependent on cluster ion size over the range $13 \leq n \leq 15$. The cluster ions with sizes $9 \leq n \leq 13$ have similar time scales for absorption recovery. The time scale for absorption recovery in $I_2^-(CO_2)_{15}$ is similar to that of $I_2^-(CO_2)_{16}$. Since dissociation occurs on a repulsive potential, recombination and vibrational relaxation must account for the transient response. Cluster ion rotation could contribute to this observed time dependence; however, experiments with pump and probe pulses polarized perpendicularly suggest that the time scale for rotational averaging is longer than that for absorption recovery.[42]

The MC and MD simulations suggest an interesting mechanism through which the transient behavior might be explained. Both models show that CO_2 molecules first cluster around the I_2^- waist to form a solvent cylinder. Within this cylinder the products of I_2^- photodissociation can undergo large-amplitude motion along the internuclear axis. This type of large-amplitude motion was observed in MD calculations on $Br_2^-(CO_2)_n$ cluster ions.[113,114] During this large-amplitude motion, one or more of the CO_2 molecules associated with the solvent cylinder around I_2^- could slip between the dissociating iodine atoms, thereby creating a solvent-separated pair and hindering recombination. However, the addition of CO_2 molecules in "capping" positions with increasing n will significantly restrict the iodine atom motion along the internuclear axis, forcing the iodine atoms to remain a contact pair. Under these circumstances, solvent intervention is unlikely, and the time required for recombination would be diminished. Based on this model, the sudden change in observed absorption recovery time could be due to the formation of singly and/or doubly capped structures in the size range $13 \leq n \leq 15$. If this picture is correct, then the 10-ps recovery time observed in $I_2^-(CO_2)_{15}$ and $I_2^-(CO_2)_{16}$ reflects the time scale for vibrational relaxation of the recombined I_2^-, while the additional time required for absorption recovery in the smaller cluster ions reflects the recombination time of the solvent-separated pair. Further experiments are required before the validity of this interpretation can be established.

In any case, the time scale for absorption recovery observed in these cluster ions is extremely fast when compared to that observed for I_2 photodissociation/geminate recombination in condensed phases. There are many possible explanations for the differences in absorption recovery times. For example, the evaporative mechanism through which internally excited cluster ions cool permits irreversible flow of energy out of the cluster ions. In condensed phases, vibrational energy transfer from the I_2 oscillator to the bath is reversible, since this energy is localized in the nearby solvent allowing energy to flow from the solvent back into the iodine bond. Vibrational relaxation in the cluster ions may also be enhanced by the near resonance of the I_2^- vibrational frequency ($113\ cm^{-1}$)[127] near the bottom of its ground-state well with the lattice vibrations of solid CO_2 ($\approx 100\ cm^{-1}$).[152]

IV. Conclusions

We have carried out photodissociation studies of $I_2^-(CO_2)_n$ cluster ions at 720 nm by using a tandem time-of-flight mass spectrometer in which the primary ion beam is mass selected in the first stage of analysis and photofragment ions are mass analyzed in a second time-of-flight stage employing a single field reflectron. Cross-section measurements indicate that I_2^- is the near-infrared chromophore in these cluster ions and that its electronic structure is not significantly perturbed by CO_2 solvation. Examination of the photofragment ions produced with a nanosecond laser pulse indicates that two types of fragment ions are generated: I^--based photofragment ions, $I^-(CO_2)_m$ ($m < n$), and I_2^--based photofragment ions, $I_2^-(CO_2)_k$ ($k < n$). Calorimetric arguments based on the typical binding energy of a CO_2 molecule to these cluster ions indicate that the photodissociated I_2^- chromophore has recombined in the I_2^--based photofragment ions and that the vibrational energy of the recombined I_2^- has largely been transferred to the solvent bath. Nanosecond photofragmentation experiments demonstrate that the quantum yield for recombination, or "caging fraction", is strongly dependent on cluster ion size over the range $0 \leq n \leq 22$. Essentially no caging is observed for $n \leq 5$, while complete caging occurs for $n \geq 16$. The caging fraction increases smoothly across the intermediate size range, $6 \leq n \leq 15$.

This size-dependent caging fraction prompted us to investigate the time-resolved dynamics of the photodissociation/geminate recombination process in these mass-selected cluster ions. Preliminary studies using picosecond pump–probe spectroscopy demonstrated the existence of very different transient bleaching responses in $I_2^-(CO_2)_9$ and $I_2^-(CO_2)_{16}$.[42] This transient bleach was modeled by using a single-exponential absorption recovery, giving time scales of 30 ± 10 and 10 ± 5 ps for $I_2^-(CO_2)_9$ and $I_2^-(CO_2)_{16}$, respectively. A single laser pulse scheme for extracting absorption recovery times was developed to survey trends in the relative recovery times across the size regime $9 \leq n \leq 16$. These single laser pulse experiments demonstrate that the absorption recovery times are slow (≈ 30 ps) for $9 \leq n \leq 13$ and fast (≈ 15 ps) for $n = 15$ and $n = 16$. This sudden shift in absorption recovery time may indicate a change in the mechanism of recombination or vibrational relaxation in cluster ions of this size. Monte Carlo and molecular dynamics simulations[115] of these cluster ions suggest that the appearance of CO_2 molecules in "capping" positions along the I_2^- internuclear axis may be responsible for limiting the range of motion experienced by the iodine atoms, thereby accelerating the recombination process. Additional experimentation will be required to verify this mechanism.

Future studies will be aimed at investigating the roles of rotational averaging and vibrational relaxation in the transient bleaching behavior of these cluster ions. Time-resolved pump–

(152) Schnepp, O.; Jacobi, N. *Adv. Chem. Phys.* **1972**, *22*, 205.

probe studies across this cluster ion size range will provide model-independent values for the absorption recovery time. Pump-probe experiments with parallel and perpendicular polarization of the laser pulses will be employed to determine the time scale for rotational reorientation in these systems and to determine its contribution, if any, to the observed transient bleaching response. Finally, two-color pump-probe studies should indicate the time scale for vibrational relaxation of the vibrationally excited I_2^- which is generated during geminate recombination. This series of experiments will permit us to evaluate the contribution of each of these processes to the observed size dependence of the absorption recovery time.

Acknowledgment. We are pleased to acknowledge a number of stimulating discussions with Professors Francois Amar, James Lisy, and Robert Parson concerning the Monte Carlo simulations. Professor Gustav Gerber provided valuable expertise in the generation and characterization of picosecond laser pulses. Monte Carlo calculations presented here were carried out on the JILA VAX 6440. This research is supported by NSF Grants PHY90-12244 and CHE88-19444.

Registry No. I_2^-, 12190-71-5; CO_2, 124-38-9.

State-Selected Photodissociation of the $B^1\Pi_u$ State of K_2 by All-Optical Triple Resonance Spectroscopy

Jiaxiang Wang, He Wang, Paul D. Kleiber, A. Marjatta Lyyra,† and William C. Stwalley*,‡

Center for Laser Science and Engineering and Department of Physics and Astronomy, University of Iowa, Iowa City, Iowa 52242 *(Received: February 20, 1991; In Final Form: May 7, 1991)*

The state-selected photodissociation of K_2 has been studied by all-optical triple resonance spectroscopy using three single-mode CW dye lasers. In particular, the positions and widths of transitions $K_2(X^1\Sigma_g^+, v'' = 17, J'') + h\nu \rightarrow K_2^*(B^1\Pi_u, v' = 43, J' = 10\text{-}43)$ corresponding to excitation of quasibound resonances in the photodissociation of K_2 have been studied. For low J' (10-28) the photodissociation was indirectly observed by studying the molecular fluorescence $K_2^*(B^1\Pi_u, v' = 43, J') \rightarrow K_2(X^1\Sigma_g^+, v'' = 60, J'') + h\nu_m$, while for high J' (20-43), the photodissociation was directly observed by studying the $K^*(4p\ ^2P_{3/2})$ atomic fluorescence $K_2^*(B^1\Pi_u, v' = 43, J') \rightarrow K^*(4p\ ^2P_{3/2}) + K$ and $K^*(4p\ ^2P_{3/2}) \rightarrow K(4s\ ^2S_{1/2}) + h\nu_a$. Predictions of both decay processes using a $B^1\Pi_u$ potential curve based on the work of Heinze and Engelke (*J. Chem. Phys.* **1988**, *89*, 42) agree well with observations.

Introduction

In recent years, we have studied the photodissociation dynamics of the $B^1\Pi_u$ state of K_2 as a model system for understanding photodissociation above and through (by tunneling) an asymptotic barrier.[1,2] These experiments involved both measurements of the photodissociation cross section and of the polarization of the atomic fluorescence, but both measurements are of thermally averaged quantities involving thousands of thermally populated quantum states. These measurements agree reasonably well with semiclassical[2] and quantum mechanical[3] calculations. Here we report the first step in providing these measurements in a state-selected rather than thermally averaged way, namely, state-selected photodissociation via tunneling quasibound states (orbiting resonances) through the asymptotic barrier. We are now seeking to extend that to state-selected measurements of other portions of the photodissociation cross section and also to the polarization of atomic fluorescence produced. We are motivated by the expectation, as discussed below, that the quasibound states will produce dramatic variations in polarization.

In particular, the measured wavelength dependence of the thermally averaged photodissociation cross section (in a thermal molecular beam at 620-640 K) agrees very well with a theoretical quantum mechanical calculation based on experimental RKR potentials.[4] More importantly, the measured wavelength dependence of the polarization of the atomic fluorescence produced by the photodissociation agrees well with two different theoretical calculations.[2,3] One calculation is a fully quantum mechanical close-coupling calculation.[3] The other calculation is semiclassical[2] and assumes that the dissociation proceeds adiabatically from small distance (Hund's case a) to intermediate distance (Hund's case c) and then in a sudden approximation to large distance (Hund's case e), after which polarized atomic fluorescence of $K^*(4p\ ^2P_{3/2})$ occurs. One interesting result of the semiclassical theory is that the polarization of photodissociation through a specific $B^1\Pi_u$ continuum level characterized by E and J is a function only of the rotation angle $\alpha(E,J)$ during dissociation (Figure 1). The rotation angle $\alpha(E,J)$ can be expressed as

$$\alpha(E,J) = \int_{R_0}^{R_L} \left[\frac{\hbar^2(J(J+1)-\Omega^2)}{2\mu R^2}\right]^{1/2} \left[E - V(R) - \frac{\hbar^2(J(J+1)-\Omega^2)}{2\mu R^2}\right]^{-1/2} \frac{dR}{R} = \int_{R_0}^{R_L} \left[\frac{E_{ROT}(R)}{E_{KIN}(R)}\right]^{1/2} \frac{dR}{R} \quad (1)$$

where E is the continuum state energy, J is the total angular momentum (rotational plus electronic, excluding nuclear spin), $\Omega = 1$ is the magnitude of the projection of the electronic angular momentum on the diatomic axis, $V(R)$ is the $B^1\Pi_u$ potential energy curve, and $E_{ROT}(R)$ and $E_{KIN}(R)$ are the local rotational and kinetic energies (from the brackets on the preceding line). The integration is carried out from the inner classical turning point R_0 to a final "locking" radius R_L, beyond which the molecular axis is no longer followed by rotation of the electronic cloud. Dynamical calculations demonstrate a negligible rotational coupling, consistent with the limit $R_L \rightarrow \infty$. Because of the barrier of 298 ± 10 cm^{-1} in the $B^1\Pi_u$ state,[4] the asymptotic kinetic energy is considerable for most states involved in the thermally averaged

† Present address: Department of Physics, Temple University, Philadelphia, PA 19122.
‡ Also Department of Chemistry.

(1) Zafiropulos, V.; Kleiber, P. D.; Sando, K. M.; Zeng, X.; Lyyra, A. M.; Stwalley, W. C. *Phys. Rev. Lett.* **1988**, *61*, 1485.
(2) Kleiber, P. D.; Wang, J.-X.; Sando, K. M.; Zafiropulos, V.; Stwalley, W. C. Photodissociation of K_2 ($X^1\Sigma_g^+$-$B^1\Pi_u$). *J. Chem. Phys.*, in press.
(3) Dubs, R.; Julienne, P. S. *J. Chem. Phys.*, in press.
(4) Heinze, J.; Engelke, F. *J. Chem. Phys.* **1988**, *89*, 42.

0022-3654/91/2095-8040$02.50/0